

CHAPTER 4

FLOOD DETECTION AND MONITORING USING MICROWAVE REMOTE SENSING

4.1 INTRODUCTION

As discussed in chapter 2, a number of techniques using microwave remote sensing exist for flood detection and monitoring purposes. However, many of them fail to give proper results with decent accuracy in places having large open water bodies and large forest area [1]. However, floods occurring at frequent intervals of time, causing the submergence of land and also posing risk to lives show the need to identify the flood prone areas in order to practice some measures to control the flood [4]. Identification of geographical extent of the area that is precarious to flood is one of the measures to alleviate the damage that is caused by flood [5]. Flood detection and monitoring are therefore considered to be very important aspects and need detailed study. Especially the use of microwave range of remote sensing in such a study is of utmost necessity.

The electrical parameter which affects all the microwave measurements is dielectric constant [2], as explained in chapter 1. The high dielectric constant makes the existing microwave remote sensing methods erroneous in places having large forest and permanent water bodies. Hence there is need of development of techniques which would be less affected by large dielectric constant value and would be more sensitive to changes in water

cover over soil. This chapter presents three new methods, developed using both passive as well as active microwave remote sensing data. The chapter is organised as the following.

Section 4.2 presents the first flood detection and monitoring technique developed, using passive microwave brightness temperature (T_B) difference. This is followed by section 4.3, where another technique developed using passive microwave remote sensed Polarization Index (PI) for flood detection as well as monitoring is presented. The subsequent section numbered 4.4 presents the technique of use of active microwave sensed backscattering coefficient (σ°) data for the purpose. Finally the chapter is concluded in section 4.5.

4.2 FLOOD DETECTION AND MONITORING USING PASSIVE MICROWAVE BRIGHTNESS TEMPERATURE DIFFERENCE

4.2.1 Introduction

Different methodologies using microwave remote sensing have been developed for detection and monitoring of flood, by many remote sensing scientists across the globe. Testing of a number of such methodologies for some places in India shows major anomaly in the accuracy level, as compared to reported values in the literatures. Hence there is a need for developing new methodologies using passive microwave remote sensing, for achieving better accuracy in flood detection and monitoring in such places.

Based on the need as discussed, the specific objective set for the present study is to test the feasibility of using passive microwave sensed brightness temperature difference, for flood detection and monitoring. The experiments are therefore done using brightness temperature (T_B) difference computations at different frequencies, polarizations and passes of the satellite. Then all different computed T_B difference values are compared with actual flood occurrences.

4.2.2 Theoretical Background

The passive microwave radiometer sensor measured brightness temperature (T_B) value is dependent on both emissivity (e) as well as thermal temperature (T_S) of the body. The mathematical expression relating the three parameters is [8]-

$$T_B = e.T_S \quad (4.1)$$

T_B values of some frequencies such as 19 GHz and 37 GHz are more sensitive to changes in surface cover from soil to water, as compared to higher frequency values [3]. For example, T_B at 91 GHz shows very little change in its value due to change in surface cover from soil to water. This difference in sensitivity is observed because of the difference in the wavelengths of the microwaves at different frequencies. The waves with longer wavelengths get emitted from the ground, with emissivity level corresponding to the level of wetness. However, for waves with shorter wavelengths, dry and wet soils as well as a water body will have the similar level of emissivity. Hence, very less effect due to change in water content of the soil is observed in case of 91 GHz. This difference in characteristics makes it possible for remote sensing scientists to use the brightness temperature (T_B) differences for surface cover change studies from soil to water cover. Hence measurement of T_B difference can be a useful method for flood detection and monitoring in large areas.

However, the T_B difference in horizontal polarization becomes high in value not only during flooding, but also due to change in soil moisture and vegetation. Whereas, the T_B difference in vertical polarization is not as much affected by soil moisture and vegetation as it is affected by surface water cover change. This difference appears mainly due to the difference in emissivity (e) in horizontal as well as vertical polarizations, as already shown in equations 1.3, 1.4 and 1.5 in Chapter 1. Thus, the difference between T_B measured at higher frequency (T_B at 91 GHz) and that at lower frequency (T_B at 19 GHz) becomes a useful parameter in detecting and monitoring flood.

4.2.3 Equipment and Data Used

For the study of flood detection and monitoring using passive microwave brightness temperature difference values, the following equipment and data are used.

- (a) Special Sensor Microwave Imager/Sounder (SSM/I/S) brightness temperature data in 19 and 91 GHz obtained from United States Air Force Defense Meteorological Satellite Program (DMSP).
- (b) A PC with remote sensing image processing software 'Beam VISAT' obtained from European Satellite Agency (ESA).

The types of SSM/I/S data used in the present work are shown in Table 4.1.

Table 4.1 Data used in Brightness Temperature difference method

<i>Sensor</i>	<i>Data</i>	<i>Frequency</i>	<i>Polarizations</i>
Special Sensor Microwave Imager/Sounder (SSM/I/S)	Near Real Time Brightness Temperature Data	19 GHz	Horizontal, Vertical
		91 GHz	Horizontal, Vertical

4.2.4 Study Area

The study area selected for detection and monitoring of flood in the present study is the state of Jammu & Kashmir in India during September 2014. Five of the severely flood affected places of the state, considered for analysis are-

- (a) Bandipur (74.65° N, 34.41° E)
- (b) Ganderbal (74.47° N, 34.14° E)
- (c) Srinagar (74.49° N, 34.50° E)
- (d) Reasi (80.81° N, 33.08° E)
- (e) Anantnag (75.15° N, 33.73° E)

The places are shown in the map of the state of Jammu & Kashmir in Figure 4.1.

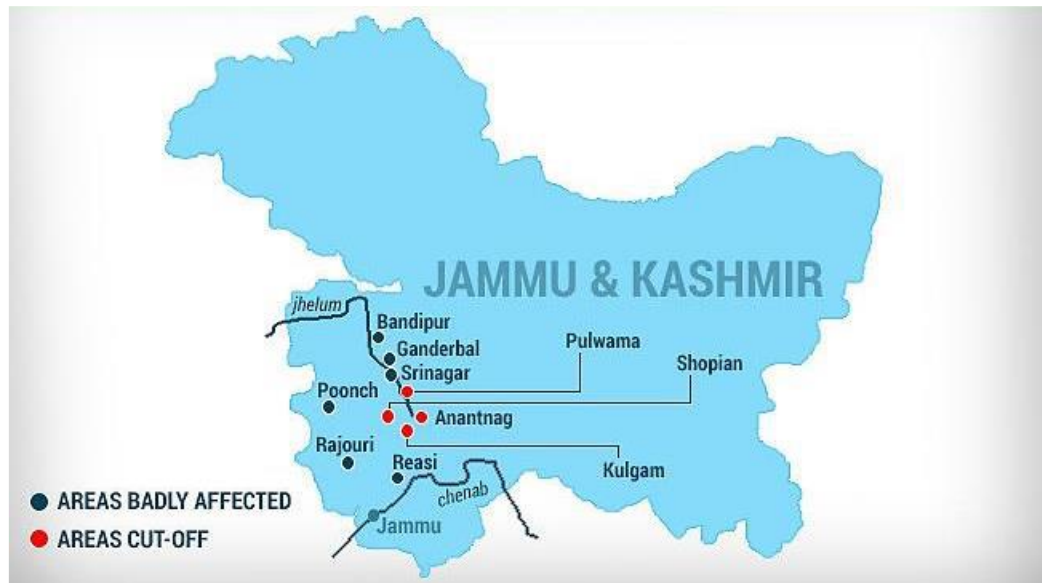


Figure 4.1: Flood affected areas of Jammu and Kashmir in September, 2014 [source: www.nrsc.gov.in]

4.2.5 Experiments done

The following experiments were done for studying the utility of the method developed.

- (1) Extracting brightness temperature (T_B) values of the study areas.
- (2) Comparison of T_B difference values computed in horizontal (H) as well as vertical (V) polarizations.
- (3) Validation of the results with flood maps of ISRO.
- (4) Calculation of accuracy level of the proposed methodology.

4.2.6 Results and Discussion

Using the methodology as discussed in the previous section, the experiments are done with the collected remote sensed data. The results of the experimentation are shown

in Figures 4.2 to 4.5. The figures show the variations of the values of T_B difference $\{T_B(19 \text{ GHz}) - T_B(91 \text{ GHz})\}$ in horizontal polarization and T_B difference $\{T_B(91 \text{ GHz}) - T_B(19 \text{ GHz})\}$ in vertical polarization computed with brightness temperature values recorded both during ascending and descending passes of the satellite respectively.

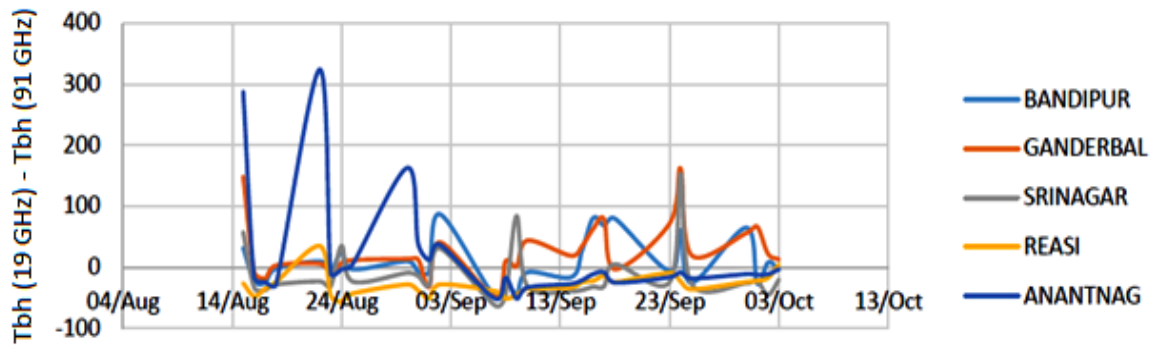


Figure 4.2: Ascending pass horizontal polarization brightness temperature difference of $\{T_B(19 \text{ GHz}) - T_B(91 \text{ GHz})\}$ for Bandipur, Ganderbal, Srinagar, Reasi and Anantnag during August-October, 2014

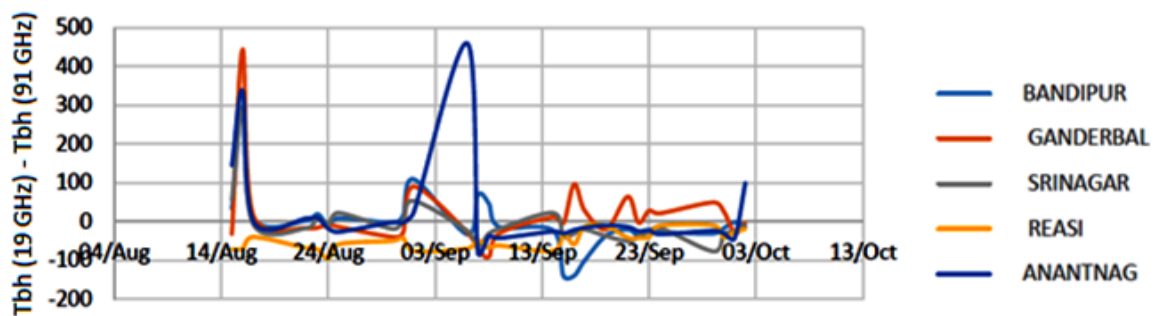


Figure 4.3: Descending pass horizontal polarization brightness temperature difference of $\{T_B(19 \text{ GHz}) - T_B(91 \text{ GHz})\}$ for Bandipur, Ganderbal, Srinagar, Reasi and Anantnag during August-October, 2014

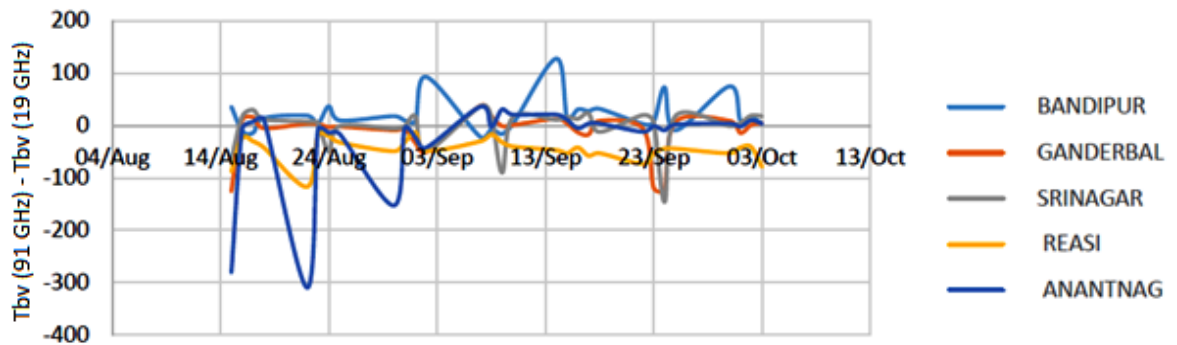


Figure 4.4: Ascending pass vertical polarization brightness temperature difference of $\{T_B(91 \text{ GHz}) - T_B(19 \text{ GHz})\}$ for Bandipur, Ganderbal, Srinagar, Reasi and Anantnag during August-October, 2014

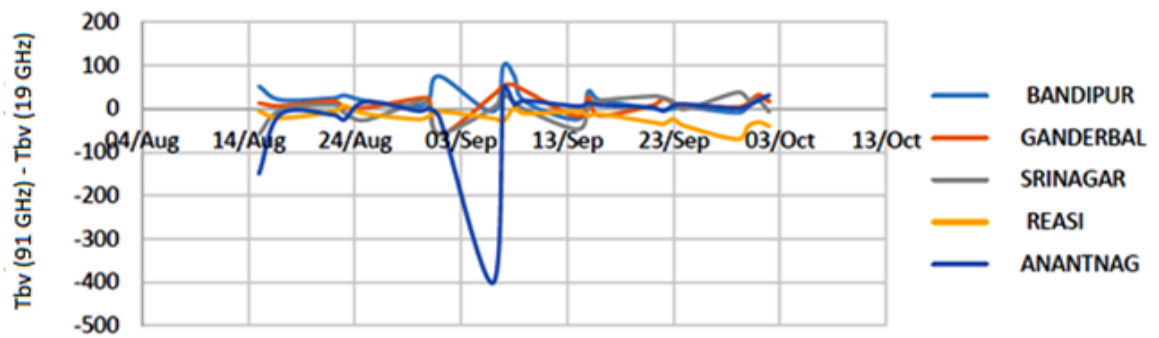


Figure 4.5: Descending pass vertical polarization brightness temperature difference of $\{T_B(91 \text{ GHz}) - T_B(19 \text{ GHz})\}$ for Bandipur, Ganderbal, Srinagar, Reasi and Anantnag during August-October, 2014

Typical values of $\{T_{Bh}(19 \text{ GHz}) - T_{Bh}(91 \text{ GHz})\}$ computed from horizontally polarized T_B values recorded during ascending pass of the satellite on a flooding date (9th September, 2014) and a non-flooding date (24th August, 2014) are compared in Table 4.2.

Table 4.2: Brightness temperature difference $\{T_{Bh} (19 \text{ GHz}) - T_{Bh} (91 \text{ GHz})\}$ values during flooding and non-flooding days

Name of the place	$\{T_{Bh} (19 \text{ GHz}) - T_{Bh} (91 \text{ GHz})\}$ values		Remarks
	9 th September 2014 (High flooding day)	24 th August 2014 (Non - flooding day)	
Bandipur	-44 K	-3 K	High negative value during flood, Very low negative value during no flood
Ganderbal	-51 K	7 K	High negative value during flood, Small positive value during no flood
Srinagar	-62 K	30 K	High negative value during flood, High positive value during no flood
Reasi	-47 K	-56 K	Not significantly different
Anantnag	-52 K	-6 K	High negative value during flood, Very low negative value during no flood

From Table 4.2 it is observed that the brightness temperature difference values $\{T_{Bh} (19 \text{ GHz}) - T_{Bh} (91 \text{ GHz})\}$ show significantly negative value during high flooding days and show either low negative or positive values during non-flooding days. However, for another flooded location Reasi, the value has not changed much from flooding to non-flooding condition. Computation of accuracy level shows an error of about 40 percent in the measurement. Experimentation and validation of the same methodology for other places in India also show an error of 40-50 percent range.

Table 4.3: Brightness temperature difference $\{T_{Bv}(91 \text{ GHz}) - T_{Bv}(19 \text{ GHz})\}$ values during flooding and non-flooding days

Name of the place	$\{T_{Bv}(91 \text{ GHz}) - T_{Bv}(19 \text{ GHz})\}$ values		Remarks
	9 th September 2014 (High flooding day)	24 th August 2014 (Non- flooding day)	
Bandipur	103 K	25 K	High positive value during flood, Low positive value during no flood
Ganderbal	67 K	- 2 K	High positive value during flood, Small negative value during no flood
Srinagar	48 K	- 36 K	High positive value during flood, High negative value during no flood
Reasi	40 K	1 K	High positive value during flood, Low positive value during no flood
Anantnag	63 K	-1 K	High positive value during flood, Very low negative value during no flood

As seen from Table 4.3, the brightness temperature difference $\{T_{Bv}(91 \text{ GHz}) - T_{Bv}(19 \text{ GHz})\}$ values change with the change in surface cover by water. From non-flooding to flooding condition, the change is towards the positive values. The T_B difference becomes more positive during flood, as compared to non-flooding condition. This acts as a reliable indication of flood. However there is an error of about 20% in detection of flood in this method.

The results of the new method proposed for flood monitoring, by measuring the difference between the T_B measured at 91 GHz and 19 GHz at vertical polarization are shown in Figures 4.4 and 4.5. More positive values in the graphs indicate flood and less positive as well as negative values indicate non-flooded conditions. The high positive

values obtained as per the graph match with the dates of actual flooding, as validated with Bhuvan data. This shows that SSMI/S T_B at 19 and 91 GHz at both polarizations can be used as a tool to detect flood. In the present context the method using vertically polarised brightness temperature data show more accuracy in detecting and monitoring flood, as noted from the validation results explained in the next sub-section.

4.2.7 Validation of the experimental results

The results obtained by the three methods are compared with the flood maps obtained from Bhuvan portal as shown in Figure 4.6. The coordinates of the flooded areas are obtained from the online image, with flooded areas shown as light blue patches on it. Then the results obtained from the experimentation are compared with the flood images of Bhuvan.

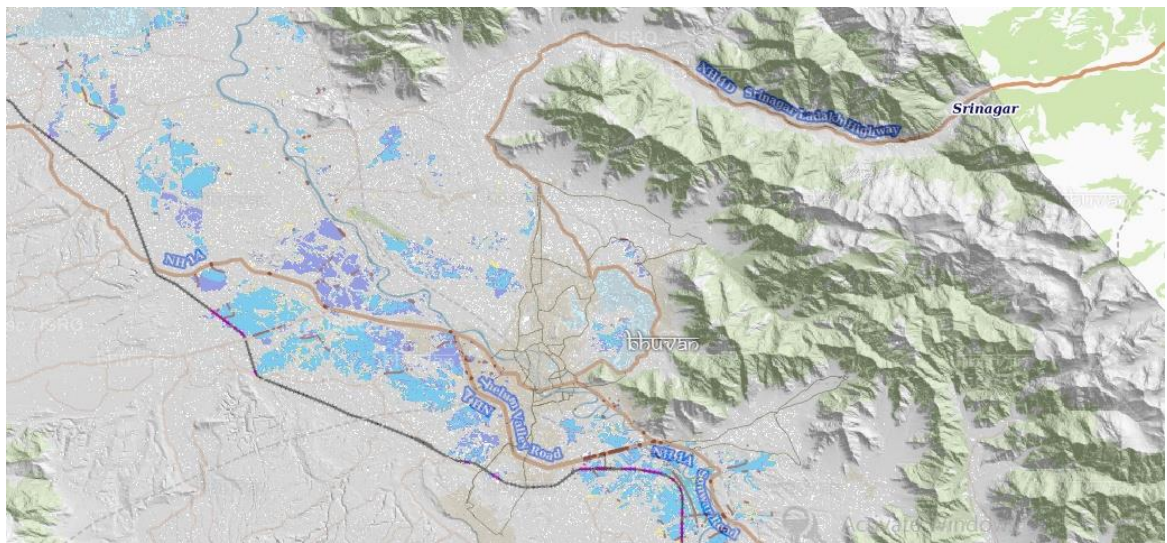


Figure 4.6: Bhuvan flood image of flood progression during 8-9 September 2014 in the study area

The exact coordinates of the area affected by flood in Bhuvan maps can be determined by taking the cursor over the light blue patches. In the online image, the longitude and latitude of the area over which the cursor is placed appear on the lower right corner of the screen. Thus the exact locations of flooding as per Bhuvan maps can be

determined. A comparison of the areas indicated as flooded areas as per the developed methodology and the area of flooding as per Bhuvan map leads to the accuracy calculations as the following.

The over estimation of flooded area in case of passive microwave remote sensed methods is an unavoidable problem, due to the low spatial resolution (25 km X 25 km) of passive microwave images. The over-estimated pixels are shown for vertically polarised T_B difference values in Figures 4.7 for a reported flooded day.

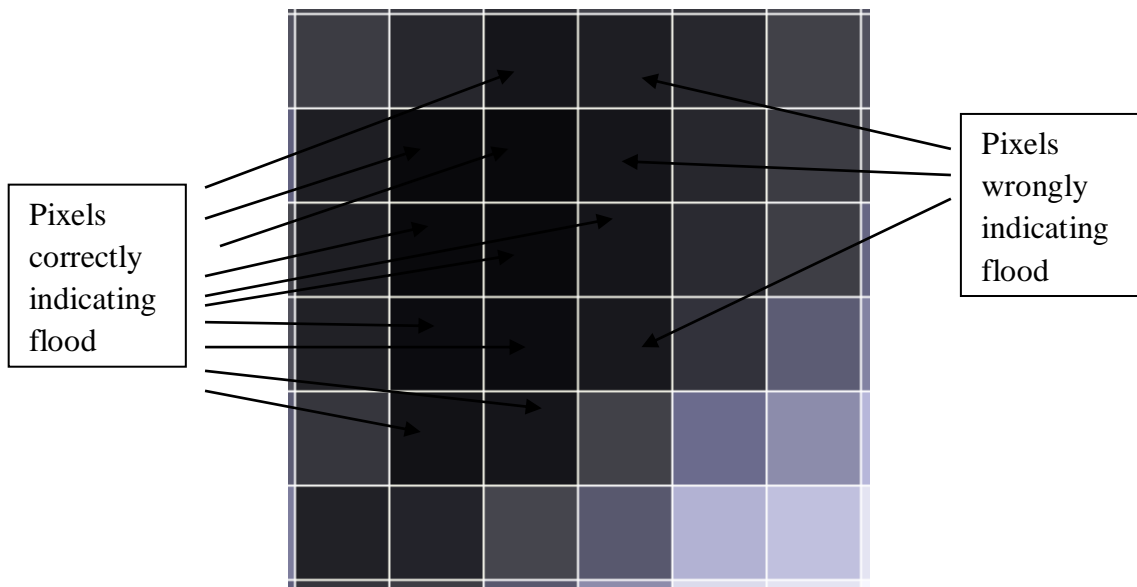


Figure 4.7: Pixel-wise analysis of flood indicated by passive microwave remote sensed brightness temperature difference method

Accuracy of the method is thus calculated based on the correct and wrong number of pixels identified as flooded areas, while using the proposed method. For figure 4.7 the accuracy calculations can be done as in the following.

Let,

The number of pixels correctly indicating flood = n_c

The number of pixels wrongly indicating flood = n_w

Then,

$$\text{Percentage Accuracy} = \frac{n_c}{n_c + n_w} \times 100$$

From the figure,

$$n_c = 10$$

$$n_w = 3$$

$$\text{Therefore, percentage accuracy} = \frac{10}{10+3} \times 100 = 76.9 \%$$

Thus, from calculations as shown above, the accuracies can be obtained for the two brightness temperature based methods, while using them for flood detection and monitoring.

- (a) Accuracy of flood detection and monitoring using T_B difference in Horizontal polarization $\{T_{Bh}(19 \text{ GHz}) - T_{Bh}(91 \text{ GHz})\} < 60\%$.
- (b) Accuracy of flood detection using T_B difference in Vertical polarization $\{T_{Bv}(91 \text{ GHz}) - T_{Bv}(19 \text{ GHz})\} > 70\%$.

A comparison of the results shown in Tables 4.2 and 4.3 show that the area called Reasi is indicated as flooded on 9th September 2014 while using the newly developed method of T_B difference computed in vertical polarization. But the existing method using T_B difference in horizontal polarization does not indicate so. As per Bhuvan map the Reasi area was flooded on 9th September 2014. This validates the greater accuracy of the newly developed method in detecting and monitoring flood.

4.2.8 Inferences

From the analysis of the brightness temperature difference (ΔT) values obtained from SSMI/S brightness temperature data for the flood events of Jammu & Kashmir in 2014, it is found that ΔT values at vertical polarization given more accurate indication of flood. The accuracy levels obtained are-

Accuracy of flood detection using ΔT in Horizontal polarization < 60 percent.

Accuracy of flood detection using ΔT in Vertical polarization > 70 percent.

Hence, for places having open water bodies, like rivers and lakes, the ΔT computed in Vertical polarization is found to be more accurate in detecting and monitoring flood.

4.3 FLOOD DETECTION AND MONITORING USING PASSIVE MICROWAVE REMOTE SENSING BY INTRODUCING A THRESHOLD TO BRIGHTNESS TEMPERATURE RATIOS

4.3.1 Introduction

The use of Brightness temperature difference and polarization difference for flood detection and monitoring give effective results in places having less open water bodies, less vegetation and low value of soil moisture. However, for places like the North Eastern states of India in general and the state of Assam in particular, these methods are not very effective. In such places, the method of Brightness Temperature ratio is also found to be not very effective. The accuracy levels of the traditional methods of flood detection and monitoring for such places having large open water bodies, vegetation and high value of soil moisture, are found to be less than 70%. Therefore there is a need for finding some alternative method for improving the accuracy level of flood detection and monitoring using microwave remote sensing.

Based on the need of developing some alternative methodologies for flood detection and monitoring in places having large open water bodies, dense vegetation and high soil moisture, the objectives of the present study are set as the following.

- (a) To test the methodology of flood detection and monitoring using brightness temperature ratio, for places having large open water bodies.
- (b) To modify the methodology as required, for obtaining greater accuracy in flood detection and monitoring, in places having large open water bodies.

- (c) To validate the modified methodology with the authentic data for establishment of the same for accurate detection and monitoring of flood.

4.3.2 Theoretical Background

Microwave brightness temperature (T_B) varies with the type of land surface cover. The value of T_B for places having no flood typically remains in the same level during a particular season. However, when flood occurs, the T_B decreases with the extent of water cover over land surface. Therefore, taking a higher land as reference, a ratio is computed as the following.

$$T_B \text{ ratio} = \frac{T_B \text{ of the place of which flood detection \& monitoring is done}}{T_B \text{ of the reference location}} \quad (4.2)$$

Here, the T_B value of the reference location changes slightly with the ambient surface temperature. However, the value of T_B for the place of study will change as per real condition of flood. When flood occurs, the T_B decreases, due to low emissivity of water, as compared to soil. Therefore, the T_B ratio would also decrease in case of flood. Thus T_B can be used for flood detection and monitoring in large areas.

4.3.3 Equipments and Data used

The following equipments and data are used in the present study.

(a) Brightness temperature data in 37 GHz from Special Sensor Microwave Imager / Sensor (SSM/I/S) radiometer in both Horizontal and Vertical polarizations, obtained from United States Air Force Defense Meteorological Satellite Program (DMSP).

(b) A PC with remote sensing image processing software 'Beam VISAT', obtained from European Satellite Agency (ESA).

4.3.4 Study Area

The data images used for this study are acquired for one whole year from October-2012 to September-2013 for Dhemaji District of Assam, India. Dhemaji district is the eastern most district of the state in the north bank of the river Brahmaputra, bounded between the Arunachal hills and the Brahmaputra River. The district is about 160 km in length and an average of 25–30 km wide with a total area of 3237 sq. km. The main rivers of the district are Kumatia, Jiadhal, Moridhal, Gai, and Simen. The gradient of the district is about 40 m from the base of the Arunachal hills to the river Brahmaputra. Ever since the great earthquake of 1950 in this region, Dhemaji has been affected by floods during every monsoon season.

4.3.5 Experiments Done

A case study from October 2012 to September 2013 on Dhemaji district of Assam, India is done with the brightness temperature (T_B) ratios obtained for measured and calibrated places. The ratios computed for the same days are used for discriminating the flooded and non-flooded areas effectively. In comparison to conventional methods used in flood monitoring, the proposed method is more accurate, even for areas with high soil moisture and large open water bodies. However, when the experiment is done with a large set of brightness temperature data and by analyzing the accuracy of the method, it was found that the method can be more effective with specific threshold values set for the different places. Thus the experimentation uses a threshold value of the T_B ratio, calculated at 37 GHz, for detection of flooding and non-flooding conditions of a particular place.

The methodology for flood detection in Dhemaji district of Assam in the year 2013 is based on the scheme as shown in the Figure 4.8, which provides a detailed overview for all the processing modules of flood extraction algorithm. The flood detection algorithm consists of two inputs; the first input consists of brightness temperature images of target area and the second input consists of brightness temperature images of reference place for calibration. Then that brightness temperature of the first input, i.e., T_{B1} and brightness temperature of the second input, i.e., T_{B2} are extracted. After that the T_{B1}/T_{B2} values are to

be plotted for different dates over the year. This graph is then analysed and the pattern of variation of the same over time is observed.

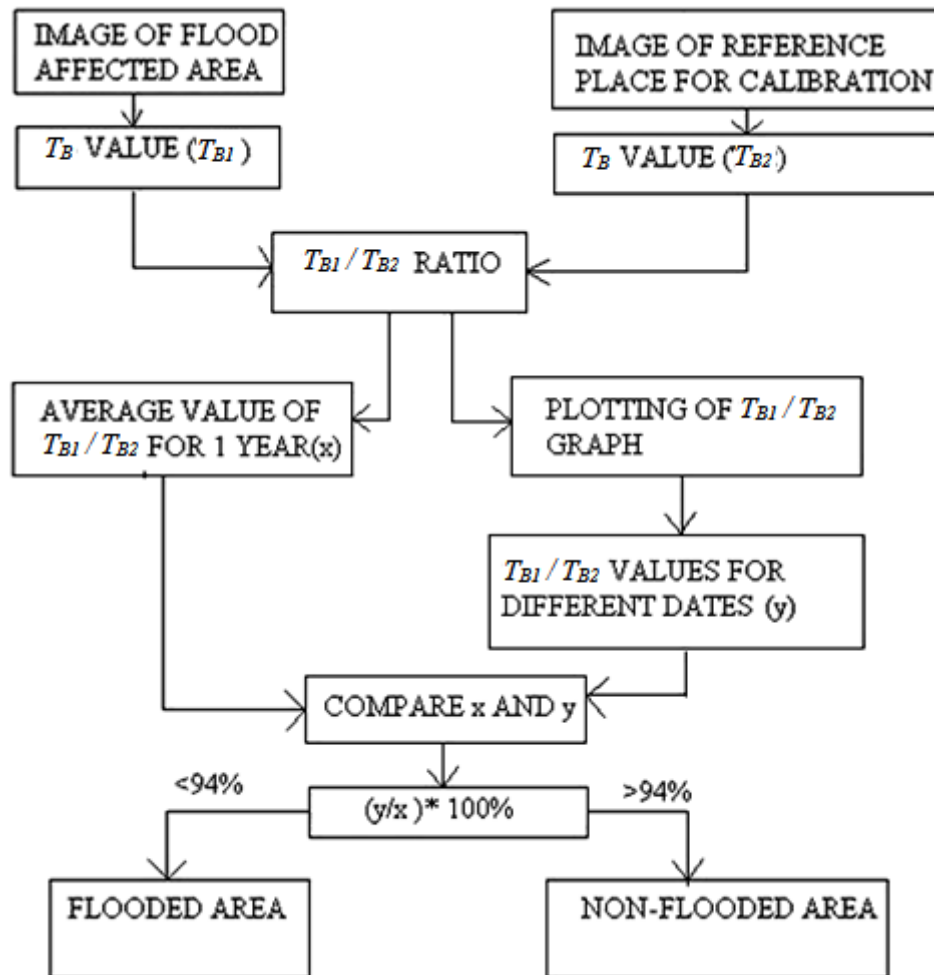


Figure 4.8: Methodology of flood detection & monitoring using T_B ratio

4.3.6 Results and Discussion

In the year 2013, as per the records in the government website of the district administration, www.dhemaji.nic.in, flood was the highest in the district of Dhemaji on 8th and 28th of July 2013. The Table 4.4 shows the brightness temperature values as well as the brightness temperature ratio values as proposed in the methodology for different places in the district. The brightness temperature measured over the place called Bordoloni had severe flood during July 2013. The places called Nari and Likabali are reference places used for calibration purpose, where flood did not occur in 2013.

Table 4.4: Brightness temperature values and ratios at 37 GHz in horizontal polarization during descending Passes for the areas in Dhemaji district

Date	Bordoloni T_{B1} (K)	Nari T_{B2} (K)	Likabali T_{B3} (K)	T_{B1}/T_{B2}	T_{B1}/T_{B3}
02-10-2012	273.1	269.1	269.7	1.0148	1.0126
10-10-2012	268.9	261.1	261.5	1.0298	1.0282
20-10-2012	257.7	257.5	256.3	1.0007	1.0054
07-11-2012	265.4	266.7	265.9	0.9951	0.9981
05-12-2012	262.6	258.5	260.3	1.0158	1.0088
16-12-2012	258.4	257.9	295.2	1.0019	0.9969
16-01-2013	258.4	265.6	260.6	0.9728	0.9915
24-01-2013	255.8	265.7	259.2	0.9627	0.9868
05-02-2013	261.6	267.5	258.9	0.9779	1.0104
16-02-2013	268.1	271.9	267.5	0.986	1.0022
28-02-2013	269.2	271.3	266.4	0.9922	1.0105
09-03-2013	266.5	271.7	265.1	0.9808	1.0052
17-03-2013	269.8	273.1	268.7	0.9879	1.004
25-03-2013	265.4	272.5	265.7	0.9739	0.9988
02-04-2013	260.7	274.8	265	0.9486	0.9837
17-04-2013	260.1	274	262.5	0.9492	0.9908
20-04-2013	258.1	275.9	264.8	0.9354	0.9746
28-04-2013	265.6	277.6	267.2	0.9567	0.994
05-06-2013	266.1	276.6	269.7	0.962	0.9866
10-06-2013	263.5	275.8	266.5	0.9554	0.9887
28-06-2013	254.3	280	264.1	0.9082	0.9628
08-07-2013	248.5	278.4	272.8	0.8926	0.9109
11-07-2013	267	278.5	268.1	0.9587	0.9958
15-07-2013	258.4	277.5	261.6	0.9311	0.9877
20-07-2013	258.9	278.7	263.6	0.9289	0.9821
03-08-2013	258.8	270.7	265.9	0.956	0.9732
13-08-2013	258.5	270	265.6	0.9574	0.9732
26-08-2013	268.4	276.5	271.6	0.9707	0.9882
07-09-2013	252.1	273.4	258.2	0.922	0.9763
15-09-2013	265.2	274.2	267.7	0.9671	0.9906
22-09-2013	271.2	272.5	268.8	0.9952	1.0089

The T_B ratios for the flooding months show the values reaching much below the average value lines of 0.96 and 0.99, as seen from the graph in Figure 4.9. Hence, after analysis of various flood occurrences, the lower threshold of brightness temperature ratio value for Dhemaji district can be set, below which if the graph goes, then for that day flood can be considered to have occurred.

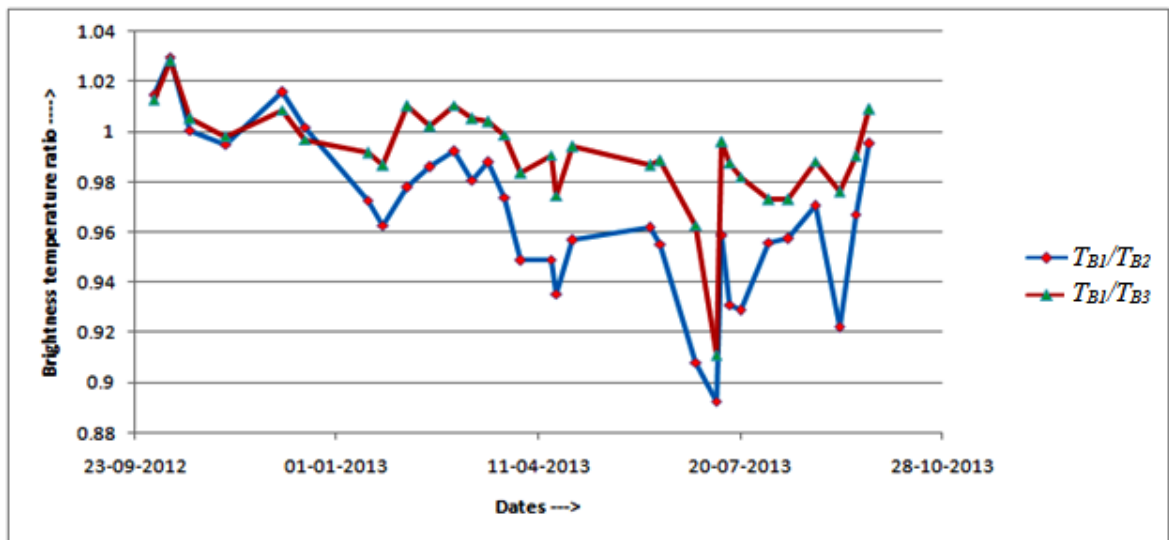


Figure 4.9: Graph of brightness temperature ratio for Bordoloni with Nari and Likabali taken as Reference

As the variations in the observed graphs occur also due to expanse of water in open water bodies, vegetation and the soil moisture, there are below-average-line values seen even on a non-flooding day. However, if the threshold of the lowest value of brightness temperature ratio is set for a particular area for actual flood identification from the graph, then it would be possible to identify flooded areas by observation from the graphs. The average value of brightness temperature ratio for Bordoloni, taking Nari as reference is found to be 0.9673 and that for Likabali as reference is found to be 0.9911. Hence, by observing the graphs, it is found that, if we set the threshold value of brightness temperature ratio for the graph as 94% below the average line for the areas in Dhemaji district, then it would show flooding and non-flooding cases clearly using the modified methodology.

With the proposed methodology, using the calculated threshold, the accuracy of detection of flood is checked for different places in the district of Dhemaji. The T_B values for three places viz., Gogamukh, Silapathar and Dipa are considered for testing the accuracy of the methodology. Likabali and Nari are the calibration places considered, as described earlier. The T_B values for the three new places along with the calibration places are shown for the period of October 2012 to September 2013 in Table 4.5.

From the table it is observed that the T_B values of Likabali and Nari do not vary much over the observed period. Hence, their selection as calibration places is found to be a correct decision. It is also observed that in comparison to the calibration places, some of the places of measurement show changes in T_B values for some period. Some places may show variations in the T_B values because of the inundation.

A graph is then plot by taking the T_B ratios of (measured place T_B) / (calibrated place T_B) in the ordinate against the dates of the concerned period in the abscissa. The variations observed in the graph are then validated with the data from authentic sources, as explained in the next section.

Table 4.5: Brightness temperature values of some areas in Dhemaji district for October 2012 to September 2013

Dates	Gogamukh T_{B4} (K)	Silapathar T_{B5} (K)	Dipa T_{B6} (K)	Nari T_{B2} (K)	Likabali T_{B3} (K)
02-10-2012	265.6	270.3	270.4	269.1	269.7
10-10-2012	265.7	266.7	265.1	261.1	261.5
20-10-2012	258	258.5	259.9	257.5	256.3
07-11-2012	261.9	263.7	269	266.7	265.9
05-12-2012	260.2	261.1	262.2	258.5	260.3
16-12-2012	255.6	257.1	261.3	257.9	295.2
16-01-2013	264.3	256.2	260.9	265.6	260.6
24-01-2013	265.1	254.1	258.7	265.7	259.2
05-02-2013	265.6	258.2	259.4	267.5	258.9
16-02-2013	271	267.2	266.3	271.9	267.5
28-02-2013	268.5	267.2	267.6	271.3	266.4
09-03-2013	270.2	265.7	266.6	271.7	265.1
17-03-2013	272.1	266.4	270.5	273.1	268.7
25-03-2013	269	264.2	266.7	272.5	265.7
02-04-2013	275.4	261.9	266.4	274.8	265
17-04-2013	273.8	255.7	265	274	262.5
20-04-2013	274.8	254.2	263.9	275.9	264.8
28-04-2013	277.8	263.5	269.9	277.6	267.2
05-06-2013	255.1	264.6	272.9	276.6	269.7
10-06-2013	253.8	258.8	269.9	275.8	266.5
28-06-2013	260.4	256.3	262.4	280	264.1
08-07-2013	277.5	254.9	261.2	278.4	272.8
11-07-2013	279.9	268.8	267.3	278.5	268.1
15-07-2013	279.2	257.7	269.2	277.5	261.6
20-07-2013	279.8	258.1	252.8	278.7	263.6
03-08-2013	277.5	258.8	262.5	270.7	265.9
13-08-2013	275.2	266.8	260.1	270	265.6
26-08-2013	275	268.4	272.7	276.5	271.6
07-09-2013	275.2	255.7	259.1	273.4	258.2
15-09-2013	275.7	265.2	273.1	274.2	267.7
22-09-2013	274.8	270.7	273.6	272.5	268.8

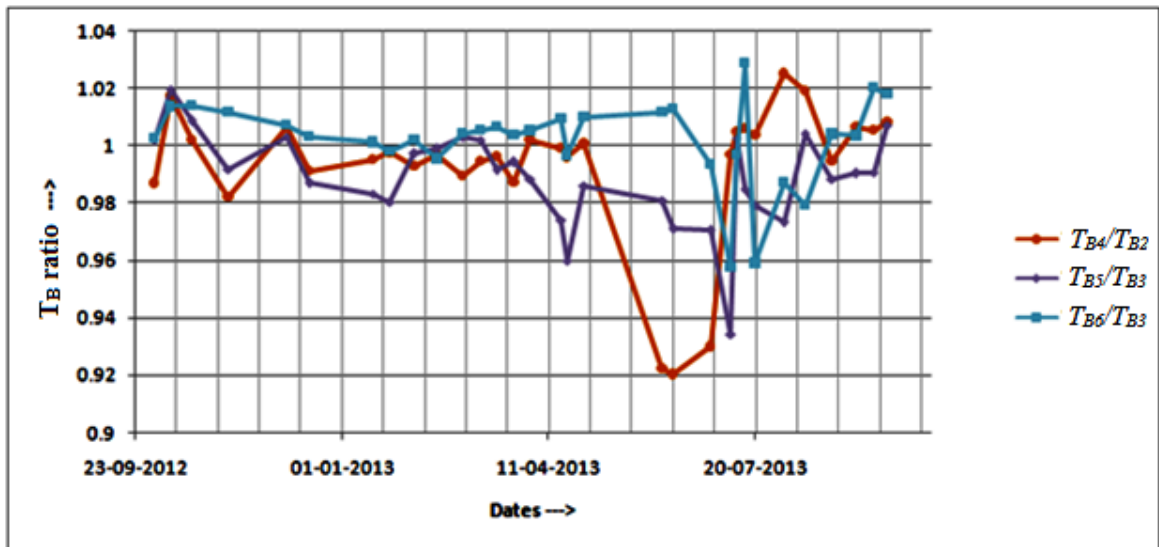


Figure 4.10: Graph of brightness temperature ratio changes for Gogamukh, Silapathar and Dipa by taking Nari and Likabali as places for calibration

4.3.7 Validation of the Experimental Results

As shown in Figure 4.10, for the place called Gogamukh in Dhemaji district, the graph goes to a steep trough. This should happen during change of surface cover, due to flood. It is also observed that for Gogamukh there was a record of flood occurrence on 28th of June 2013 as per the report of Assam State Disaster Management Authority (ASDMA). As the graph shows a value of brightness temperature ratio for that day going below the 94% of the average value of brightness temperature ratio for that place, it is indicating flood in the area.

However, in the figure it is also seen that the graph is never crossing the lower limit of 94% for Dipa and Silapathar, which shows no flooding in those places during the period of October 2012 to September 2013. In those places flood actually did not occur during the period considered, as validated with ASDMA reports. Hence, there is clear indication of flood occurrences as far as areas and dates of flooding are concerned, using the described methodology of setting a lower threshold of Brightness Temperature ratio of 94%. The modified brightness temperature ratio method is thus validated for flood detection and monitoring successfully.

The accuracy analysis of the method is done by comparing the results of the proposed methodology with the standard flood images of Bhuvan and the flood reports of ASDMA. The Figure 4.11 shows an image of the computed brightness temperature ratio, with the compared results marked as shown.

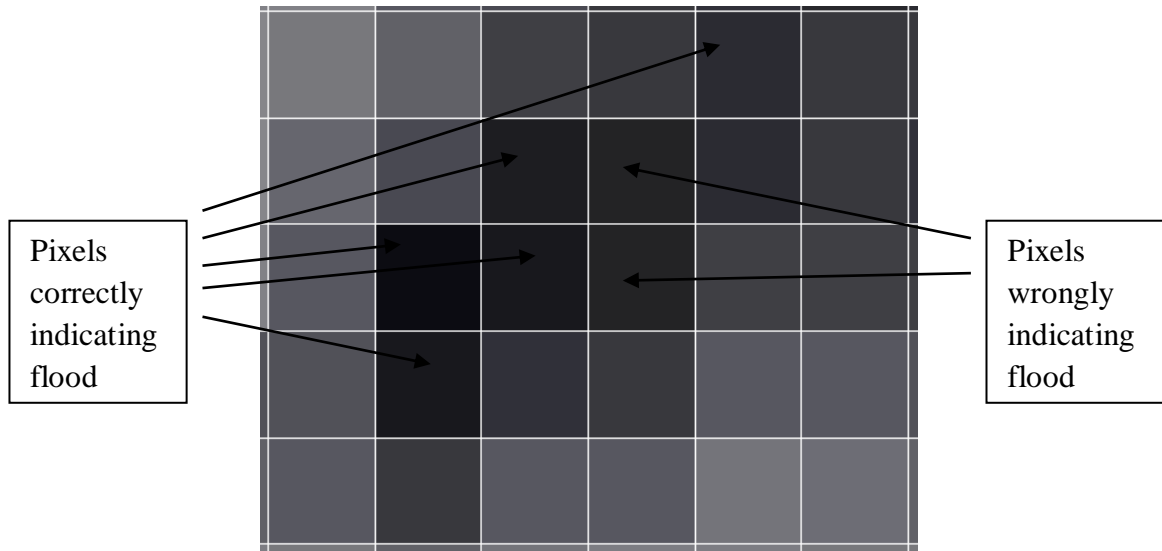


Figure 4.11: Pixel-wise analysis of flood indicated by passive microwave remote sensed brightness temperature ratio method

Accuracy of the method is thus calculated based on the correct and wrong number of pixels identified as flooded areas, while using the proposed method. For Figure 4.11 the accuracy calculations can be done as in the following.

Let,

The number of pixels correctly indicating flood = n_c

The number of pixels wrongly indicating flood = n_w

Then,

$$\text{Percentage Accuracy} = \frac{n_c}{n_c + n_w} \times 100$$

From the figure,

$$n_c = 5$$

$$n_w = 2$$

$$\text{Therefore, percentage accuracy} = \frac{5}{5+2} \times 100 = 71.4 \%$$

Such accuracy calculations are done for five different areas in the state of Assam and inferences are drawn based on the results obtained.

4.3.8 Inferences

The methodology of threshold setting for flood detection and monitoring using brightness temperature ratio is effective for areas having large open water bodies and high soil moisture. The same idea of introducing a threshold to brightness temperature ratio can be applied for detection and monitoring of flood in any place, where the simple brightness temperature ratio does not indicate real flood situations. The places having open water bodies, high soil moisture and large vegetation areas require this methodology for flood detection and monitoring.

The accuracies of the original and modified brightness temperature ratio methods for flood detection in Assam are shown in the following.

Accuracy in flood detection and monitoring using brightness temperature ratio is less than 50 percent.

Accuracy of flood detection and monitoring using brightness temperature ratio with a set threshold value is greater than 70 percent.

Thus, determination of threshold individually for different areas can help in detecting and monitoring flood effectively even in places having large open water bodies, dense vegetation cover and high soil moisture.

4.4 FLOOD DETECTION AND MONITORING USING PASSIVE MICROWAVE POLARIZATION INDEX

Polarization Index (*PI*) is a derived quantity from microwave brightness temperatures (T_B), utilised in soil moisture sensing. The use of the same quantity in detecting and monitoring flood in places with large open water bodies is experimented with. The details of the experimentation, results and validation are presented in the following.

4.4.1 Introduction

The methods described in the previous sections for flood detection and monitoring in places having large open water bodies use brightness temperature data with accuracies of about 70 percent. Therefore a need is felt to develop more accurate methods for detection and monitoring of flood occurrences using Passive microwave sensing.

Flood occurrences are closely related to soil moisture levels. Increase of soil moisture beyond saturation point leads to most of the floods. Passive microwave remote sensing is extensively used in soil moisture measurement of large areas with high temporal resolution of two times a day of data availability as mentioned already in Chapter 1. Use of bands up to 12 GHz has been done for soil moisture studies as seen from literature reviews in Chapter 2 already. One of the common methods of soil moisture measurement using passive microwave brightness temperature data is the use of polarization index (*PI*) at L (1-2 GHz), S (2-4 GHz), C (4-8 GHz) and X (8-12 GHz) bands. Hence, there was a need for studying the utility of *PI* in flood studies too, as flood is related to soil moisture.

Therefore, the present study aims at finding the suitable frequency at which the *PI* can be effective in detecting and monitoring flood in a large area.

4.4.2 Theoretical Background

As explained in Chapter 1, the polarization index (PI) shows higher value for higher value of soil moisture. This is because the brightness temperature measured in horizontal polarization (T_{BH}) decreases more than the brightness temperature measured in vertical polarization (T_{BV}) with the increase in soil moisture, hence the difference becomes high. When the land surface is covered by water due to inundation, the decrease in T_{BH} value is even more as compared to T_{BV} . This would increase the PI value further, indicating the change in the land cover from bare soil to water covered soil.

4.4.3 Equipments and Data used

In this present study of utilisation of microwave brightness temperature in determination of PI , the following equipments and data are used.

- (a) A PC with the remote sensing image processing software ‘Beam-VISAT’, obtained from European Satellite Agency (ESA).
- (b) Passive Microwave Brightness Temperature data obtained from Advanced Microwave Scanning Radiometer (AMSR) 2 sensor on board the Global Change Observation Mission (GCOM-W1) satellite of Japan Aerospace Exploration Agency (JAXA).

Figure 4.12 shows a sample brightness temperature image from AMSR 2 sensor of GCOM-W1 satellite.

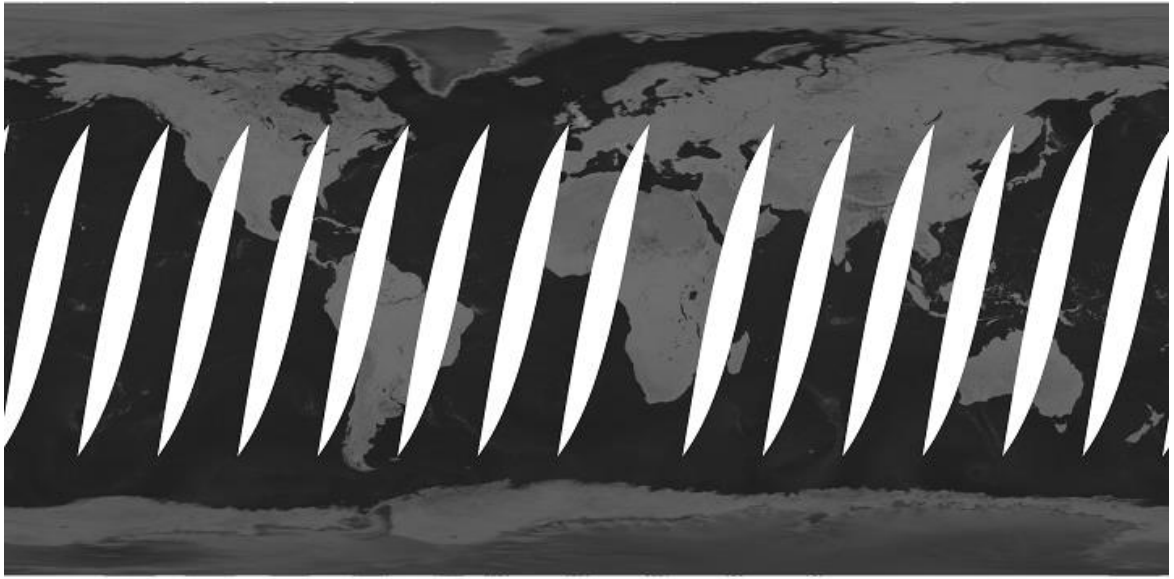


Figure 4.12: Level-3 Global Image of 10 GHz Horizontal Polarization Brightness Temperature from AMSR-2 on 11th July 2017 acquired during descending pass of GCOM-W1

A unique feature of the AMSR-2 based brightness temperature data is its regional extent. Daily global coverage of the sensor allows the creation of regional overview maps, which cannot be created with high-resolution satellite images which have smaller footprints.

4.4.4 Study Area

The brightness temperature values are obtained from the images as shown in the Figure 4.13. The pixel with its boundary longitudes and latitudes are marked in the figure. As seen from the geo-location, the centre of the pixel under study is 92.2°E longitude and 26.3°N latitude. The upper and lower boundaries are 26.35°N and 26.25°N latitudes respectively. The left and right boundaries are 92.15°E and 92.25°E longitudes respectively. The pixel area is 10 km x 10 km in size. The area covered by the pixel is in Morigaon district of the state of Assam in India. The area is shown in the map of Figure 4.14. The area concerned is highly vulnerable to flood during the monsoon season every

year. The river Brahmaputra flows through the northern side of the district, causing flood due to high flow during monsoon in its southern bank.

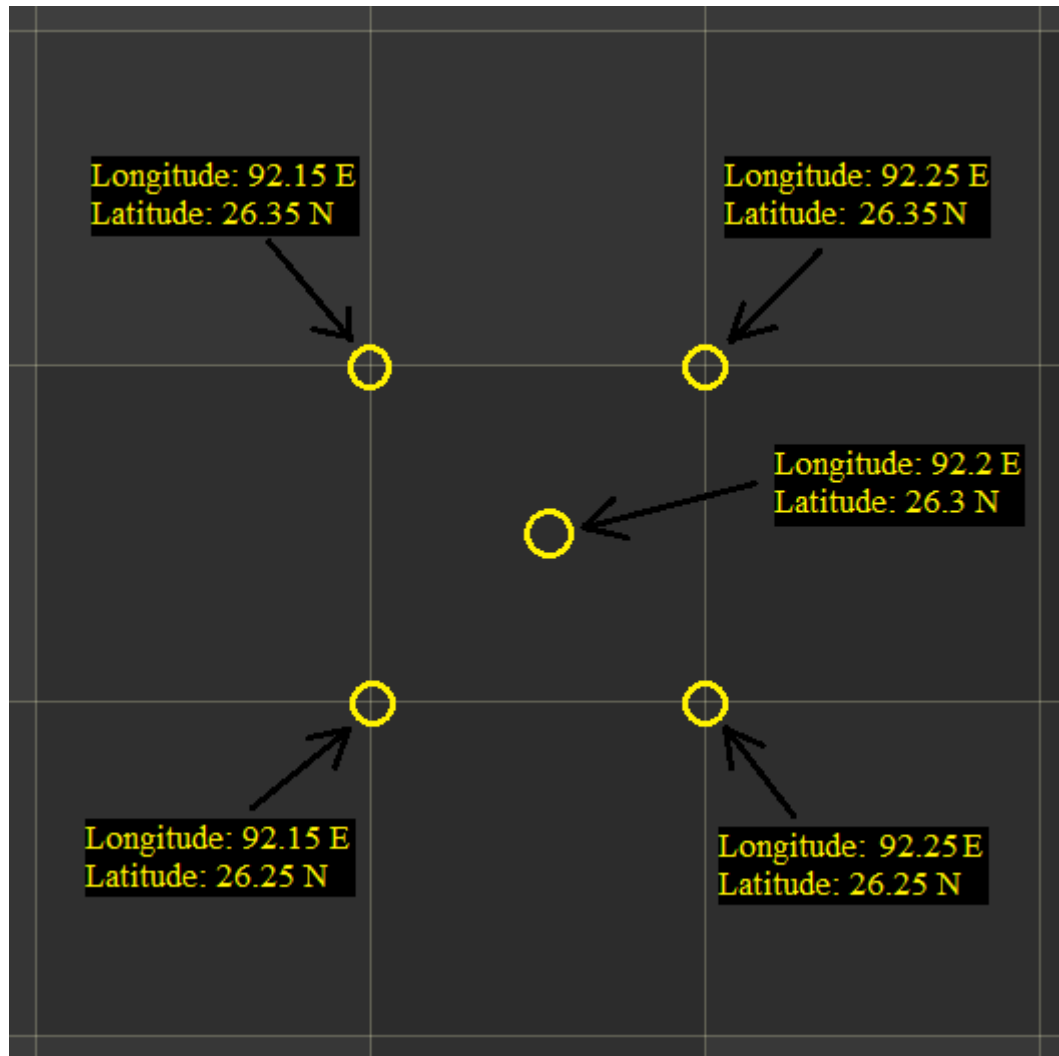


Figure 4.13: Geo-location of the pixel under study (Centre of the pixel: 92.2°E/26.3°N)



Figure 4.14: Area under study in Morigaon district of Assam for flood detection and monitoring using polarization index

4.4.5 Experiments done

The temporal variation of brightness temperature values in both horizontal and vertical polarizations are recorded from the daily images acquired during descending passes of the GCOM-W1 satellite. The Table 4.6 shows the brightness temperature values of the pixel, from 6th July to 27th July 2017.

From the brightness temperature values the polarization index (PI) values are computed. The PI values are then correlated with the flood occurrences in the area. Thus the effectiveness and accuracy of the methodology is evaluated.

The experimentation also involved determination of suitable frequency for PI computation, which will be the most sensitive to flood occurrences. The frequencies tested with are- 6, 7, 10, 18, 22 and 36 GHz respectively. The experimental results of the most suitable frequency (i.e., 10 GHz) for PI calculation for flood detection and monitoring are presented in the subsequent section.

Table 4.6: Brightness temperatures obtained at 10 GHz during descending passes from AMSR-2 sensor on board GCOM-W1 satellite

Dates of data availability	Brightness temperature in 10 GHz with horizontal polarization (K)	Brightness temperature in 10 GHz with vertical polarization (K)
6th July 2017	208.17	226.87
8th July 2017	207.63	243.98
10th July 2017	175.82	227.22
11th July 2017	166.89	221.1
13th July 2017	167.87	223.28
15th July 2017	177.97	230.51
17th July 2017	185.98	234.41
18th July 2017	190.8	237.14
19th July 2017	185.26	235.1
20th July 2017	188.06	235.69
22nd July 2017	196.17	241.03
24th July 2017	196	239.34
26th July 2017	202.76	245.74
27th July 2017	207.26	246.67

It is to be noted that for brightness temperatures of 6, 7, 18, 22 and 36 GHz, the *PI* values do not show a uniform trend of increase or decrease. However, at 10 GHz the trend is uniform, i.e., there is no abrupt change of *PI* for a particular period. Hence, 10 GHz brightness temperature data has been used for computation of *PI* and validation of results with ground truth data.

4.4.6 Results and Discussion

The *PI* values computed from 10 GHz brightness temperature data as discussed in the previous section show a temporal variation as in Figure 4.15.

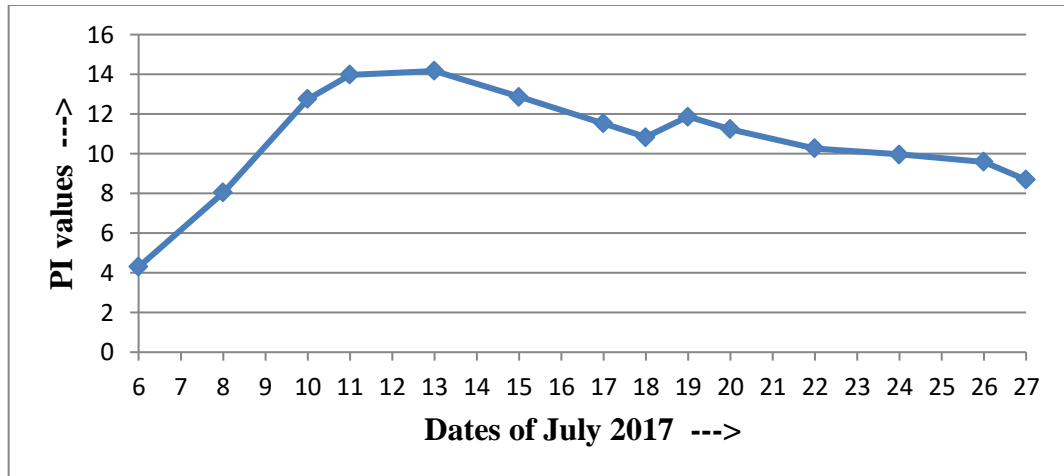


Figure 4.15: Temporal variation of *PI*

As observed from the figure, there is a sloping increase in the value from 8th July 2017 onwards. The *PI* value crosses a magnitude of 10 on 10th July 2017. The value remains high for a period from 10th July to 24th July 2017, indicating inundation in the area covered by the pixel.

4.4.7 Validation of the Experimental Results

Flood detected using *PI* based method is validated with Bhuvan flood images and Assam State Disaster Management Authority (ASDMA) daily flood reports. High flooding is reported by ASDMA in their online daily flood report portal <http://asdma.gov.in/reports.html> during the same days as the dates of high values of *PI* in the previous section. The graph of Figure 4.16 shows the crop area affected by flood during the month of July 2017 in hectares. The exactly matching dates of flooding as per ASDMA reports and the indication of flood by high *PI* values in five such areas in the state of Assam validate the method for the period of 2014 to 2017. Comparison of *PI* values with Bhuvan images also validates the high level of accuracy of the proposed method.

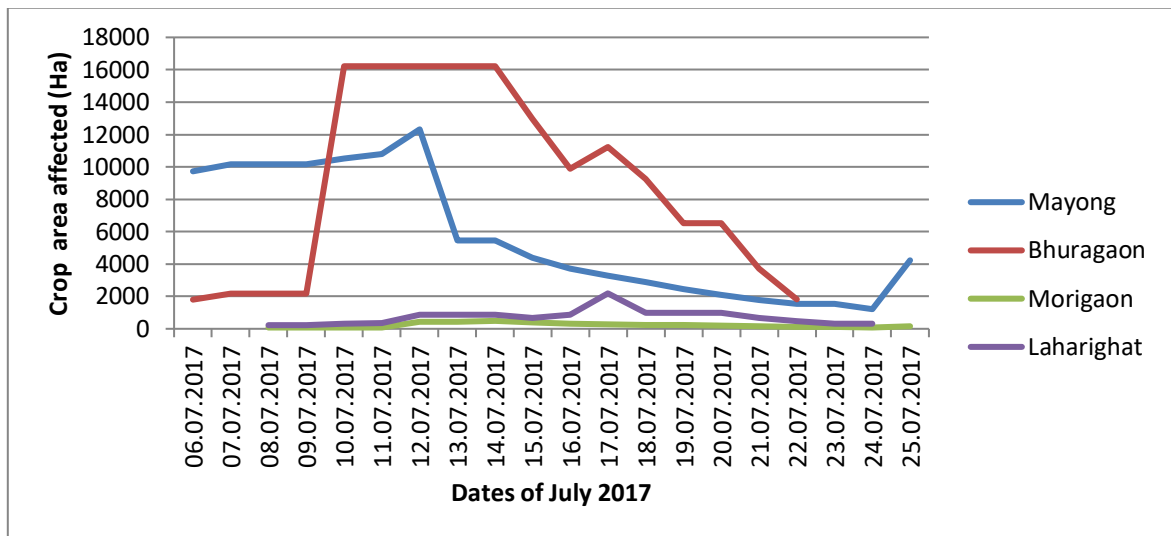


Figure 4.16: Crop area affected in the district of Morigaon in July 2017

Accuracy of the method is determined by considering number of pixels correctly and wrongly indicated as flooded in an area under consideration. The image showing correct and wrong indication due to *PI* values is shown in figure 4.17.

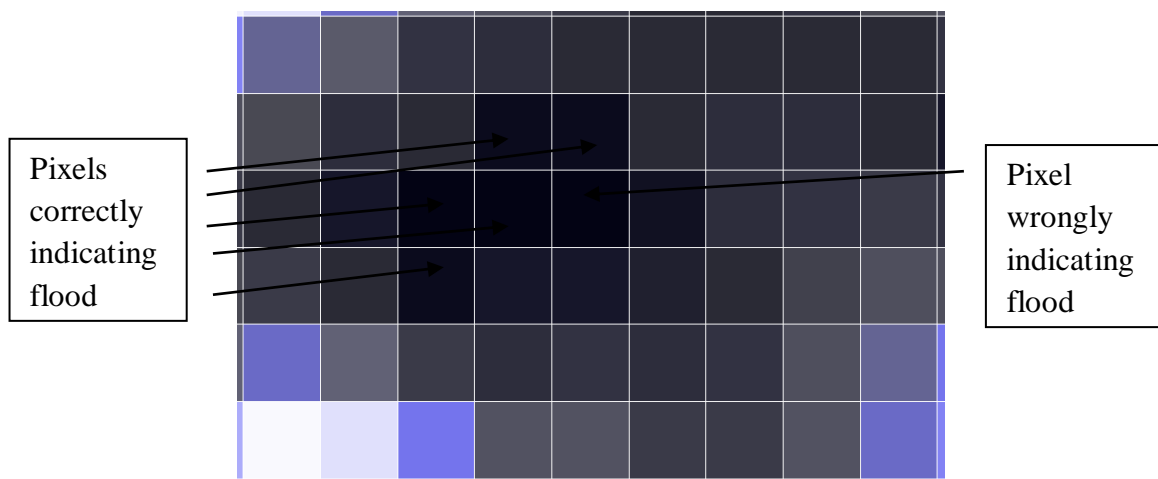


Figure 4.17: Pixel-wise analysis of flood indicated by passive microwave remote sensed polarization index method

Accuracy of the method is thus calculated based on the correct and wrong number of pixels identified as flooded areas, in comparison to Bhuvan flood image. For figure 4.17 the accuracy calculations can be done as in the following.

Let,

The number of pixels correctly indicating flood = n_c

The number of pixels wrongly indicating flood = n_w

Then,

$$\text{Percentage Accuracy} = \frac{n_c}{n_c + n_w} \times 100$$

From the figure,

$$n_c = 5$$

$$n_w = 1$$

$$\text{Therefore, percentage accuracy} = \frac{5}{5+1} \times 100 = 83.3 \%$$

Such accuracy calculations are done for many areas and inferences are drawn based on the results obtained.

4.4.8 Inferences

A very high accuracy of detection of flood is observed using microwave *PI*. The accuracy level measured based on the number of correct and wrong indications of flooded pixels in Morigaon district over a period of five years reveal more than 80 percent accuracy in flood detection and monitoring. Thus the high temporal resolution passive microwave data is found to be useful in indicating flood in areas having extensive cloud cover. However, as the size of the pixels is very large in passive microwave remote sensing, best spatial resolution being 10 km x 10 km, there is over-estimation of the flooded area always. Hence, a finer resolution study using active microwave data is needed to point to the flooding locations more precisely.

4.5 FLOOD DETECTION AND MONITORING USING ACTIVE MICROWAVE SCATTERING COEFFICIENT

Use of active microwave remote sensing in flood studies is relatively newer phenomenon, as compared to passive microwave sensing. The biggest demerit of passive sensing, i.e., coarse resolution of the images is not there in active sensing. Active sensing images have resolution up to 5 m x 5 m, in contrast to the best resolution of passive sensing images of 5 km x 5 km. Hence, active microwave sensing can be utilised for flood studies with high spatial resolution. However, as mentioned earlier, active microwave remote sensing has poor temporal resolution of 5-12 days, in contrast to passive microwave remote sensing temporal resolution of 0.5 day only.

4.5.1 Introduction

Synthetic Aperture Radar (SAR) data is used in detection and monitoring of flood, as described in this section. Following is a detailed description of the studies made on detection and monitoring of flood using active microwave SAR remote sensing. The study area, experimental details, results and validation processes are explained sequentially in subsequent sub-sections.

4.5.2 Theoretical Background

As explained in Chapter 1, the characteristics of backscattered microwave from the surface of the earth depend on the surface profile. The microwave scattering depends largely on the dielectric constant of the surface material. As explained earlier, the dielectric constant values of soil and water are significantly different; hence the backscattering coefficient value also varies hugely for soil and water. Therefore backscattering coefficient is expected to be a useful parameter in flood studies.

Also when there is flood, specular reflection from flood water causes the backscattering coefficient value to become very low. When there is no flood, the surface

scattering is due to soil and/or vegetation. The scattering due to soil or vegetation is much higher as compared to that due to water. Thus there is a marked variation of SAR backscattering coefficient observed during flood, as compared to non-flooded conditions.

4.5.3 Equipments and Data used

In the present study, SAR images from Sentinel-1A satellite of European Satellite Agency (ESA) have been used. The SAR image of the same area as covered by one pixel of Figure 4.14 of the previous section is shown in Figure 4.18.

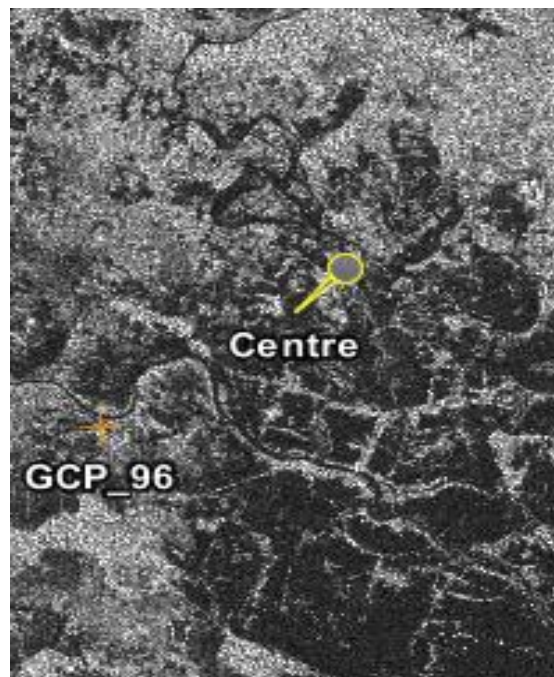


Figure 4.18: SAR image of the area under study acquired on 2nd July 2017 (Centre: 92.2°E/26.3°N)

The SAR image shows the variations of surface cover within the area. The white pixels in the image show bare land, the black pixels show water cover and the grey pixels show presence of vegetation, constructed roads, buildings, mixture of land and water bodies etc. The black pixels are due to the reflected beams away from the SAR antenna, due to specular reflection in water bodies.

In the present study, the SAR images are analysed using ‘Beam-VISAT’ image processing software, obtained freely from European Satellite Agency (ESA).

Because of high spatial resolution, the spatial variations of land cover can be monitored in greater detail in the SAR image. Thus inundation in an area in greater detail is studied using the SAR images obtained from Sentinel-1A in both VH and VV polarizations. VH polarization refers to vertically polarized transmitting antenna with horizontally polarized receiving antenna. VV polarization refers to both transmitter and receiver antenna in vertical polarization.

4.5.4 Study Areas

The study areas for experimentation are in the districts of Morigaon and Dhemaji in the state of Assam in India. The temporal as well as spatial variations of the SAR scattering coefficient values for the areas are studied. The geo-locations of the pixels under study are shown in Table 4.7 and 4.8 respectively.

Table 4.7: Geo-locations of the pixels under study in the SAR image of Morigaon district

Pixel Name	Longitude	Latitude	Ground attribute
Centre	92.20	26.30	Permanent Water Body
1	92.29	26.30	Areas inundated during the flooding period of 10 th July to 22 nd July, 2017
2	92.33	26.38	
3	92.30	26.35	High land / non-flooding area

Table 4.8: Geo-locations of the pixels under study in the SAR image of Dhemaji district

Pixel Name	Longitude	Latitude	Ground attribute
Pin 1	95.11	27.63	Flooded area
Pin 2	95.12	27.63	Non-flooded area
Pin 3	95.13	27.63	Non-flooded area
Pin 4	95.14	27.64	Flooded area
Pin 5	95.13	27.64	Non-flooded area
Pin 6	95.11	27.64	Non-flooded area

For the study in Morigaon, the pixel locations in the VH polarization images during three days, viz., 2nd July (non-flooded day), 14th July (flooded day) and 26th July (non-flooded day) are shown in Figures 4.19 to 4.21.

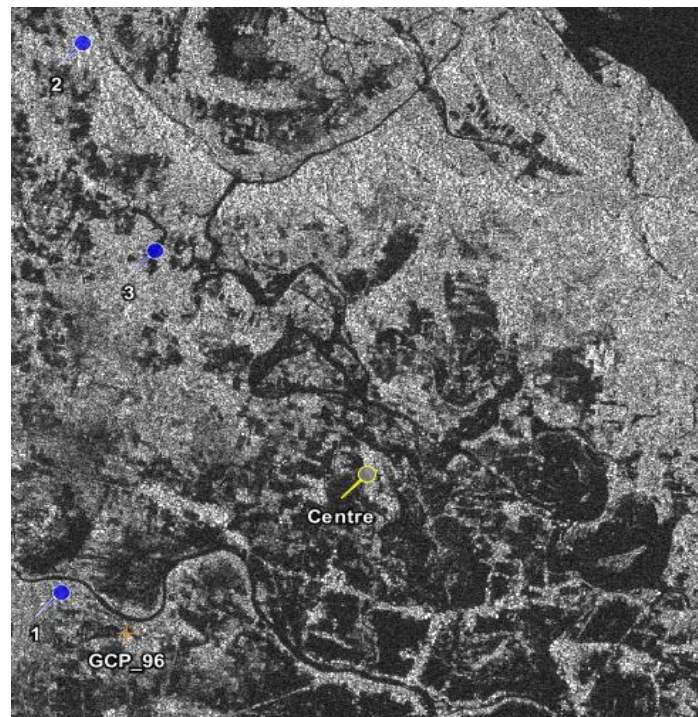


Figure 4.19: Study locations of Morigaon district on the SAR image of Sentinel 1-A in VH polarization on 2nd July 2017

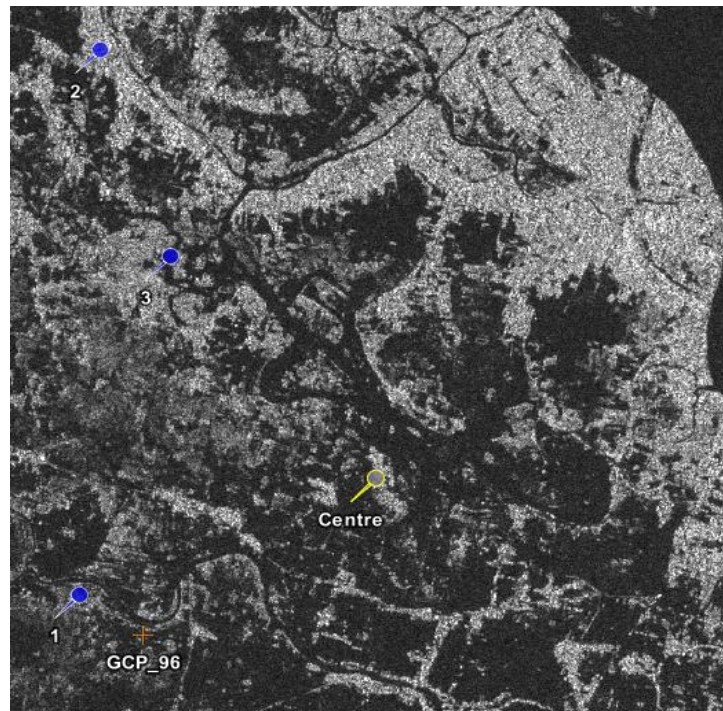


Figure 4.20: Study locations of Morigaon district on the SAR image of Sentinel 1-A in VH polarization on 14th July 2017

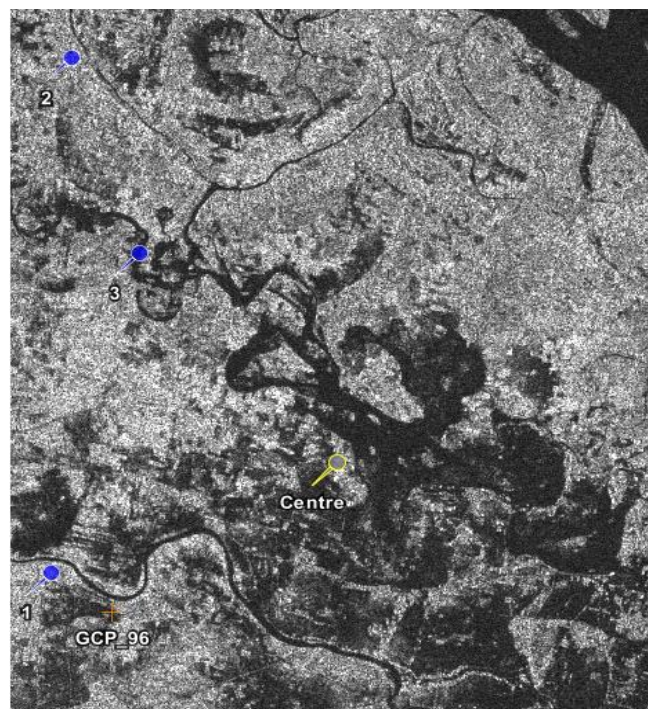


Figure 4.21: Study locations of Morigaon district on the SAR image of Sentinel 1-A in VH polarization on 26th July 2017

Similarly the pixel locations of another study area called Jonai in Dhemaji district on 26th of August 2018 are shown in Figure 4.22.

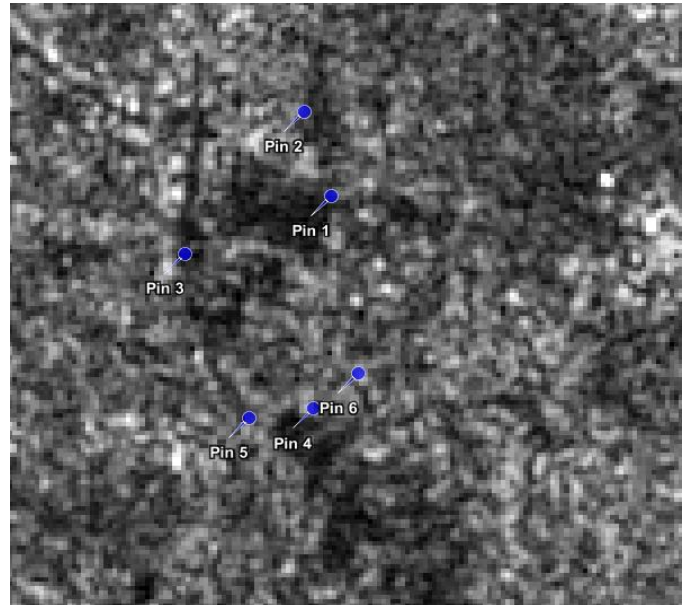


Figure 4.22: Study locations of Dhemaji district on the SAR image of Sentinel 1-A in VH polarization on 26th July 2017

Jonai reported flooding during the month of August in 2018. Hence, the study is made in that area to find the validity of the method of flood detection and monitoring as discussed in the subsequent sections.

4.5.5 Experiments Done

SAR images show the variations in the greyscale values due to scattering from the ground. In the present study, a comparison is done between SAR image greyscale value variations with respect to surface cover change for both VH and VV polarizations. Thus the spatial and temporal variations of the greyscale values in both sets of polarizations are studied to possibly correlate with flood occurrences. The greyscale values of the pixels corresponding to some known flooded and non-flooded locations are noted. Then graphs are plotted location-wise for both flooding and non-flooding days. The graphs are then

analysed for determining the correlation with the flood occurrences, both spatially as well as temporally.

This method is then validated by applying it in some other locations to establish the correlation between abnormally low value of backscattering coefficient and flood.

4.5.6 Results and Discussion

The variation of scattering coefficient values obtained for VH and VV polarizations from the SAR images of Morigaon are shown in Table 4.9 and 4.10. As seen from the tables, the scattering coefficient values of the centre pixel location and pixel location 3 do not vary much during the three days-

- (a) A day much before flood (2nd July 2017),
- (b) A day during flood in Morigaon district (14th July 2017), and
- (c) A day much after the flood (26th July 2017).

This is because the centre pixel is a part of a permanent water body and the location 3 is a high land. So, their surface scattering characteristics do not change much even during the reported flooding dates in the district.

Table 4.9: Scattering coefficient variation in different locations of Morigaon for VH polarization image of Sentinel 1A

Locations	2nd July	14th July	26th July
Centre	40	34	58
1	115	43	146
2	99	14	95
3	136	150	153

Table 4.10: Scattering coefficient variation in different locations of Morigaon for VV polarization image of Sentinel 1A

Locations	2nd July	14th July	26th July
Centre	83	39	78
1	389	69	431
2	179	82	202
3	328	295	231

From the Tables 4.9 and 4.10 it is observed that for locations 1 and 2, the scattering coefficients change significantly. It may be because of the flood occurrences in those places. The same has been confirmed with flood reports and flood maps from ASDMA and Bhuvan respectively, as described in the subsequent section.

The graphs of the variations of scattering coefficient values are shown in Figure 4.23 and 4.24.

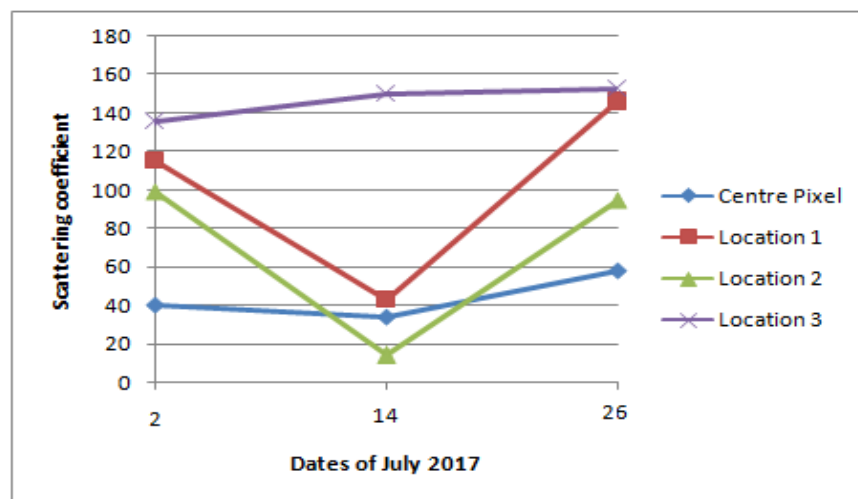


Figure 4.23: Variation of Backscattering coefficient in four places of Morigaon district in the month of July 2017 for VH polarization SAR image

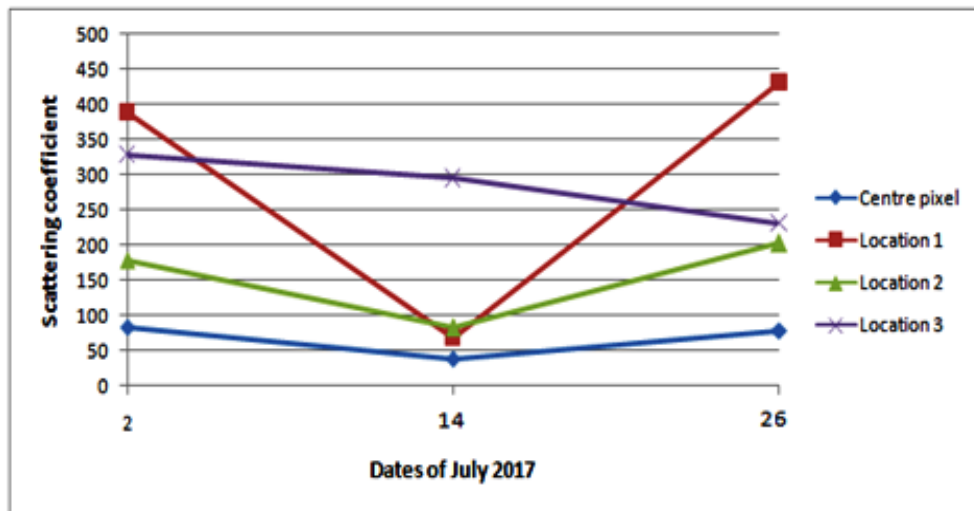


Figure 4.24: Variation of Backscattering coefficient in four places of Morigoan district in the month of July 2017 for VV polarization SAR image

From Figures 4.23 and 4.24 it is observed that the scattering coefficient variation is more significant in case of VV polarized SAR data as compared to VH polarized ones. The low value of scattering coefficient is found to be because of the specular reflection from the water surface.

Similarly the experiment is done for Jonai, where the temporal variation of backscattering coefficient is observed during the flooding period, as shown in Table 4.11.

Table 4.11: Variation of backscattering coefficient with flooding in Jonai in 2018

Locations	21 st August	26 th August	31 st August
Pin 1	154.0	42.0	140.0
Pin 2	162.0	138.0	143.0
Pin 3	148.0	174.0	157.0
Pin 4	155.0	58.0	163.0
Pin 5	147.0	116.0	150.0
Pin 6	166.0	136.0	149.0

The variations of backscattering coefficient are plotted against the dates considered for VV polarization in SAR images as shown in Figure 4.25 and 4.26. The variations are then analysed to find any correlation with the flooded areas.

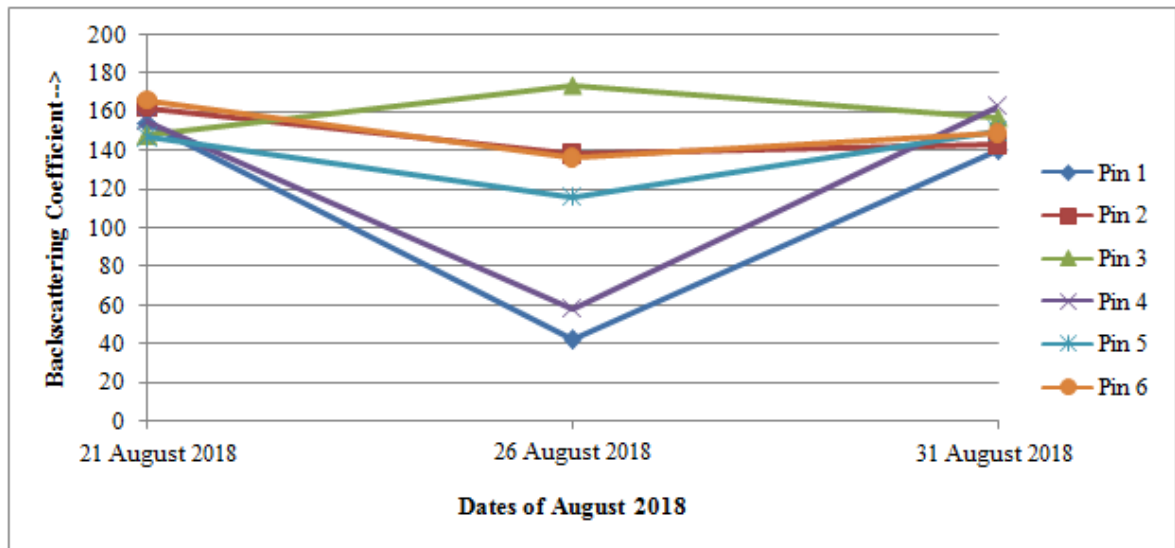


Figure 4.25: Variation of Backscattering coefficient in five places of Dhemaji district in the month of August 2018 for VV polarization SAR image

As observed from the figure, the backscattering coefficients become very low (40-60) on the SAR image of 26th August 2018 at locations marked by pin 1 and 4. For all the other locations, the backscattering values are higher in range (>100) during all the dates considered. This abnormal decrease in backscattering coefficient value may happen due to specular reflection of the microwaves from the water surface. During flood such a water surface reflects the microwaves and therefore the backscattering coefficient value decreases. Validation of the method of observation of backscattering coefficient value for flood detection and monitoring with standard data is done as explained in the following sub-section.

4.5.7 Validation of the Experimental Results

The images in Figures 4.23 and 4.24 show the prominent changes in the backscattering coefficient (σ^0) values on 14th July for the flooded pixels. The flood

locations as indicated experimentally are compared with the Bhuvan flood maps. The locations having low backscattering coefficient values (dark pixels) match exactly with those marked as flooded in Bhuvan images. Thus the flood maps of Bhuvan confirm the matching flooding dates with the experimentally found ones.

Another flood prone area in Dhemaji district called Jonai as shown in Figure 4.22 is now considered for validation of the backscattering based flood detection and monitoring method. As per ASDMA reports Jonai area in Dhemaji district was affected by flood during the period of 23rd August to 5th September 2018. When compared with Bhuvan flood map it is found that the particular areas considered (pin 1 and 4) were affected during the period of 23rd to 28th August 2018. Hence, the indication of low value of backscattering coefficient on 26th of August and high values shown on 21st as well as 31st of August are clearly differentiating between flooded and non-flooded days. The observation of backscattering coefficient in the VV SAR image is found to be more accurately indicating flooding conditions.

The accuracy calculations done are based on the observation of correctly and wrongly indicated pixels in the flooded area. One such calculation done for Jonai area is demonstrated in the following. The Figure 4.26 shows the pixels correctly and wrongly indicating flood by high greyscale value in a SAR image, as validated with the Bhuvan flood image, in August 2018.

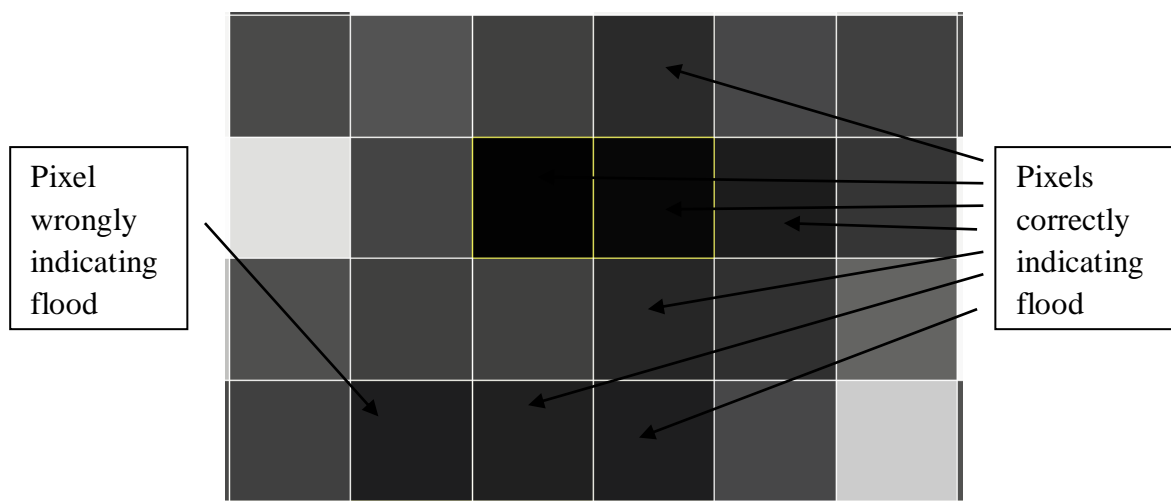


Figure 4.26: Pixel-wise analysis of flood indicated by SAR backscattering coefficient observation based method in VV polarization

Accuracy of the method is thus calculated based on the correct and wrong number of pixels identified as flooded areas, while using the proposed method. For Figure 4.14 the accuracy calculations can be done as in the following.

Let,

The number of pixels correctly indicating flood = n_c

The number of pixels wrongly indicating flood = n_w

Then,

$$\text{Percentage Accuracy} = \frac{n_c}{n_c + n_w} \times 100$$

From the figure,

$$n_c = 8$$

$$n_w = 1$$

$$\text{Therefore, percentage accuracy} = \frac{8}{8+1} \times 100 = 88.8 \%$$

Such accuracy calculations are done for many other areas also and finally inferences are drawn based on a number of results obtained.

4.5.8 Inferences

The active microwave SAR maps are found to be useful in detecting flood with a high spatial resolution of 5 m x 5 m. It is also observed that the over-estimation of flooded area as in passive microwave sensing does not happen when active microwave remote sensing is used. However it needs to be mentioned here that the availability of SAR data over a particular area is not as frequent as passive microwave data. The satellite revisit time is 5-12 days in case of active microwave satellites. Hence, a combination of both, i.e., detection of flood frequently in a large area (10 km x 10 km) using passive microwave sensing and pin-pointing the actual flooded portions (5 m x 5 m) within the flooded area using active microwave remote sensing, can be a highly useful combination.

4.6 FLOOD BOUNDARY DELINEATION USING SAR DATA

A novel study done on determination of flood boundary using active microwave remote sensed SAR data is explained in the following. The experimental details, results and validation processes are described sequentially in this section of the thesis.

4.6.1 Introduction

The flooded portions in an active microwave remote sensing image can be detected accurately, as described in the last section. However, to exactly determine the boundary of the flooded area and hence to delineate the flooded portion in the remote sensed image is of great importance. However, such a study using active microwave remote sensing has not yet been reported in any available literature. Hence, a need was felt to study this important aspect of flood boundary determination. A detailed experimentation is therefore done in this regard. What follows is a description of the process followed and results obtained thereof, in studying flood boundary delineation using active microwave remote sensing.

4.6.2 Theoretical Background

Scattering Coefficient (σ°) as explained and used in the previous section for flood detection and monitoring is useful in differentiating between soil and water cover over the earth's surface. The σ° has been extensively used in studies related to soil moisture studies also. Therefore, σ° is considered to have potential to delineate flood boundary with high spatial resolution. The greatest advantage of use of σ° in flood boundary delineation is its high sensitivity to surface cover change. The σ° for the same place changes considerably from non-flooded to flooding days.

4.6.3 Equipments and Data used

In the present study, SAR images from Sentinel-1A satellite of European Satellite Agency (ESA) have been used. The SAR images are analysed using ‘Beam-VISAT’ image processing software, obtained freely from European Satellite Agency (ESA).

4.6.4 Study Area

The area for flood boundary delineation experimentation is in the Morigaon district of the state of Assam in India. Figure 4.27 shows the selected area of study with its centre coordinates.

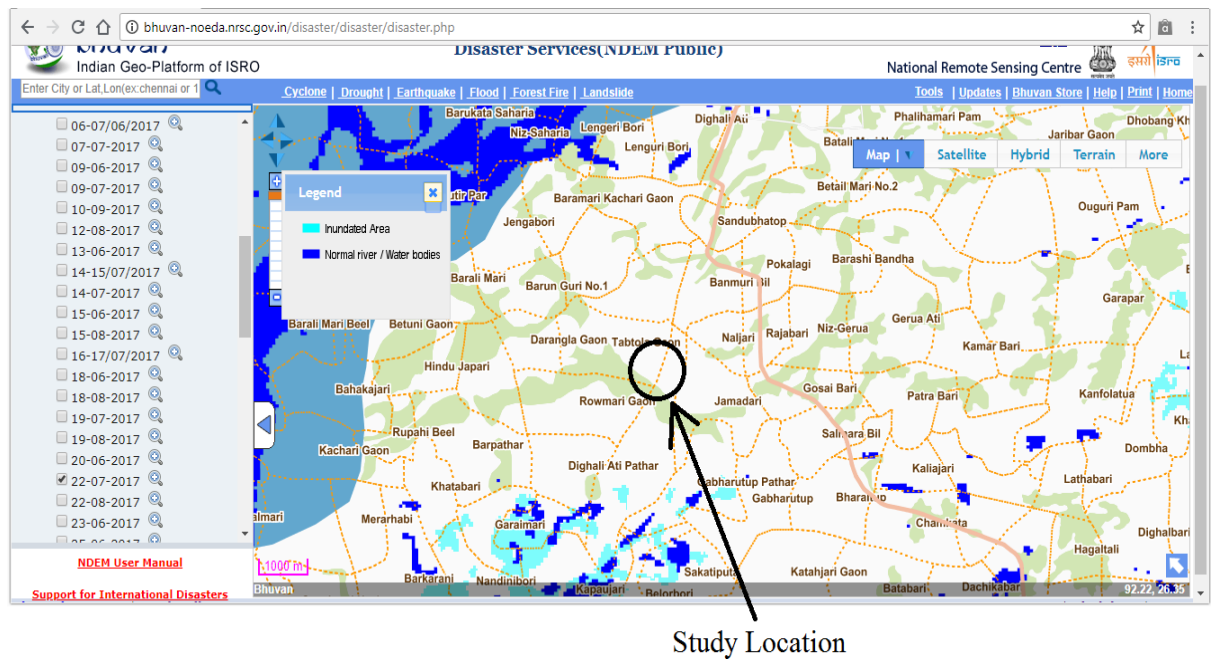


Figure 4.27: Area under study (Longitude: 92.22°E, Latitude: 26.35°N) [Map source: <http://bhuvan-noeda.nrsc.gov.in/disaster/disaster/disaster.php>]

4.6.5 Experiments done

In the present study, a comparison is done between SAR image greyscale value variations with respect to surface cover change for both VH and VV polarizations. Thus the spatial and temporal variations of the greyscale values in both sets of polarizations are studied to possibly correlate with flood boundary determination. The greyscale values of the pixels corresponding to some known flood boundary locations are noted. Then graphs are plotted for backscattering coefficient values of the flooded location from inside the flooded area to outside it, moving through the adjacent pixels. The graphs are then analysed for possible correlation of backscattering coefficient with the positions across the boundary of a flooded area.

4.6.6 Results and Discussion

Figures 4.28 to 4.33 show the area under study in the SAR images obtained from Sentinel 1A satellite, in both VH and VV polarizations. The images are of three days-

- (a) a day much before the reported flood, i.e., 2nd July 2017,
- (b) a day during the flooding, i.e., 14th July 2017, and
- (c) a day much after the flood, i.e., 26th July 2017.

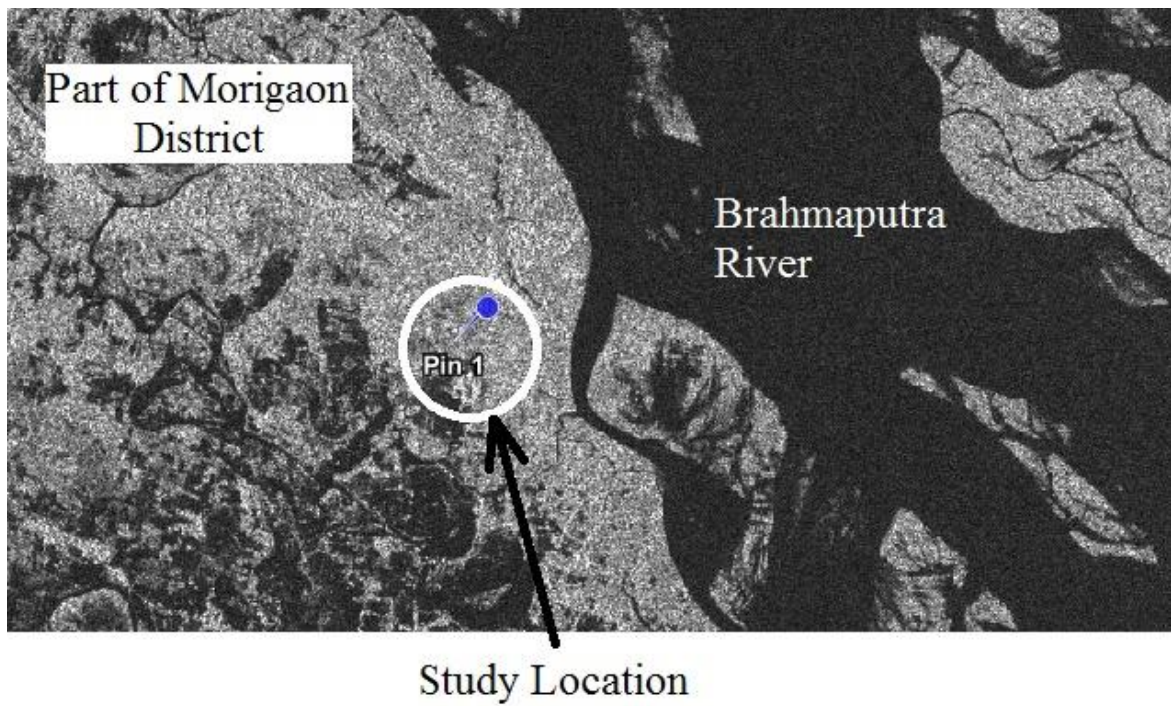


Figure 4.28: Study area before the occurrence of the flood on 2nd July 2017 as seen in a VH SAR image

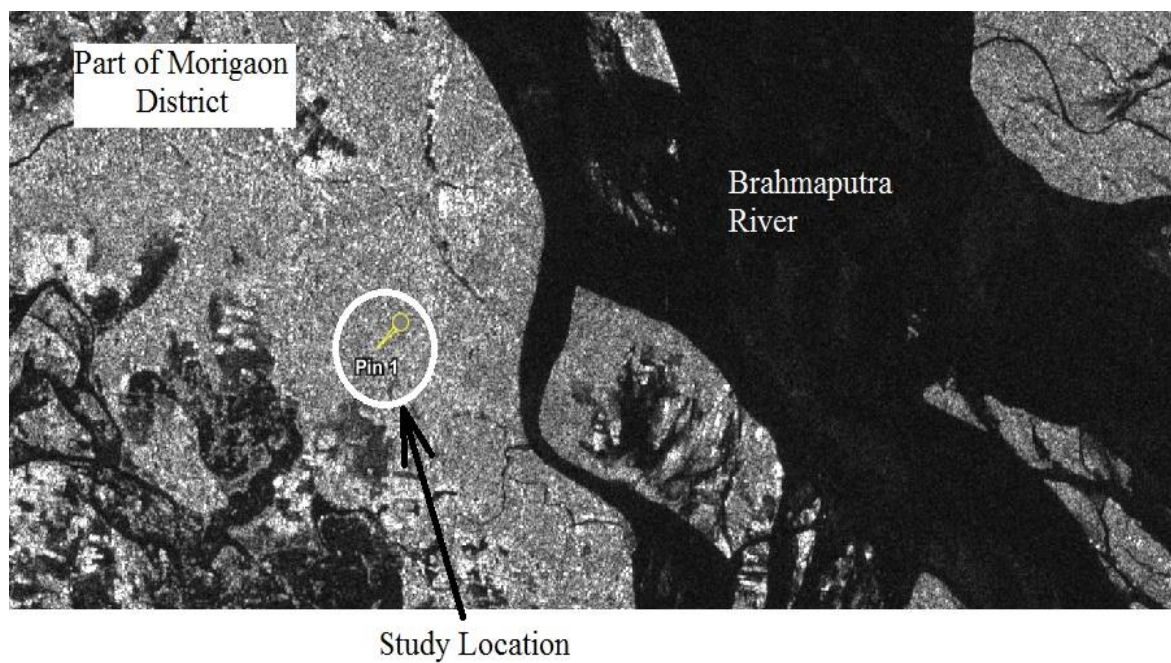


Figure 4.29: Study area before the occurrence of the flood on 2nd July 2017 as seen in a VV SAR image

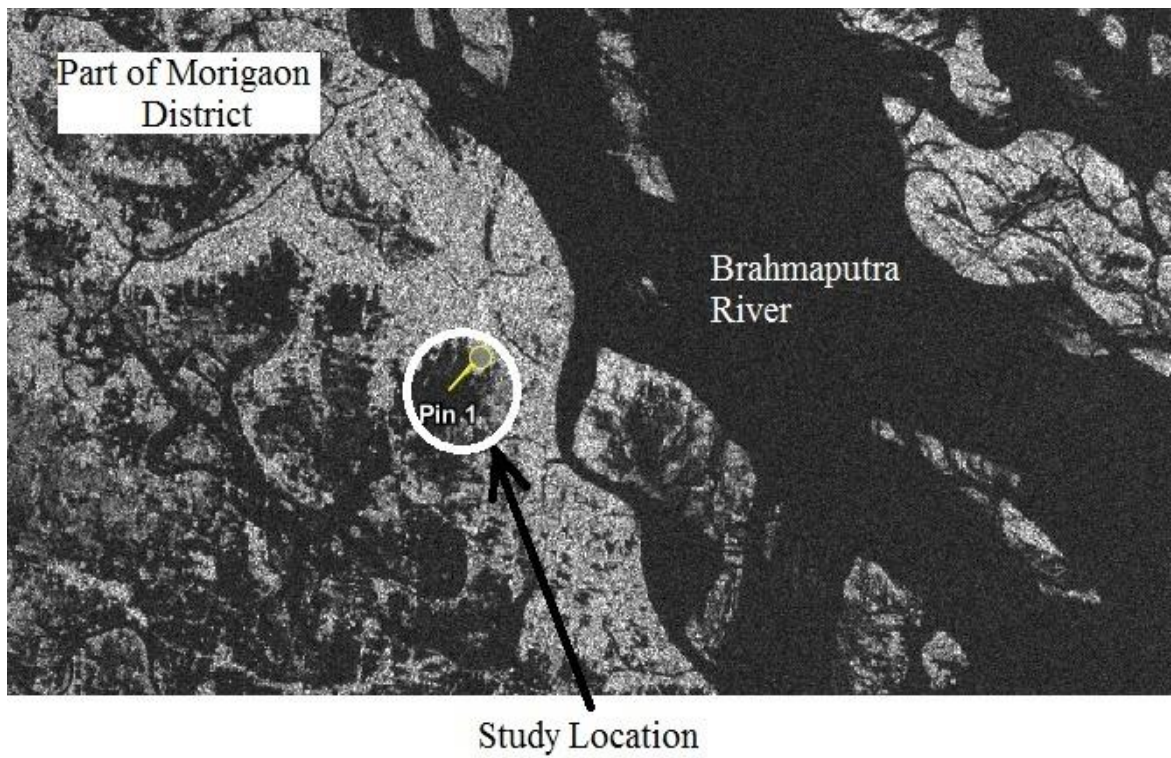


Figure 4.30: Study area during flooding on 14th July 2017 as seen in a VH SAR image

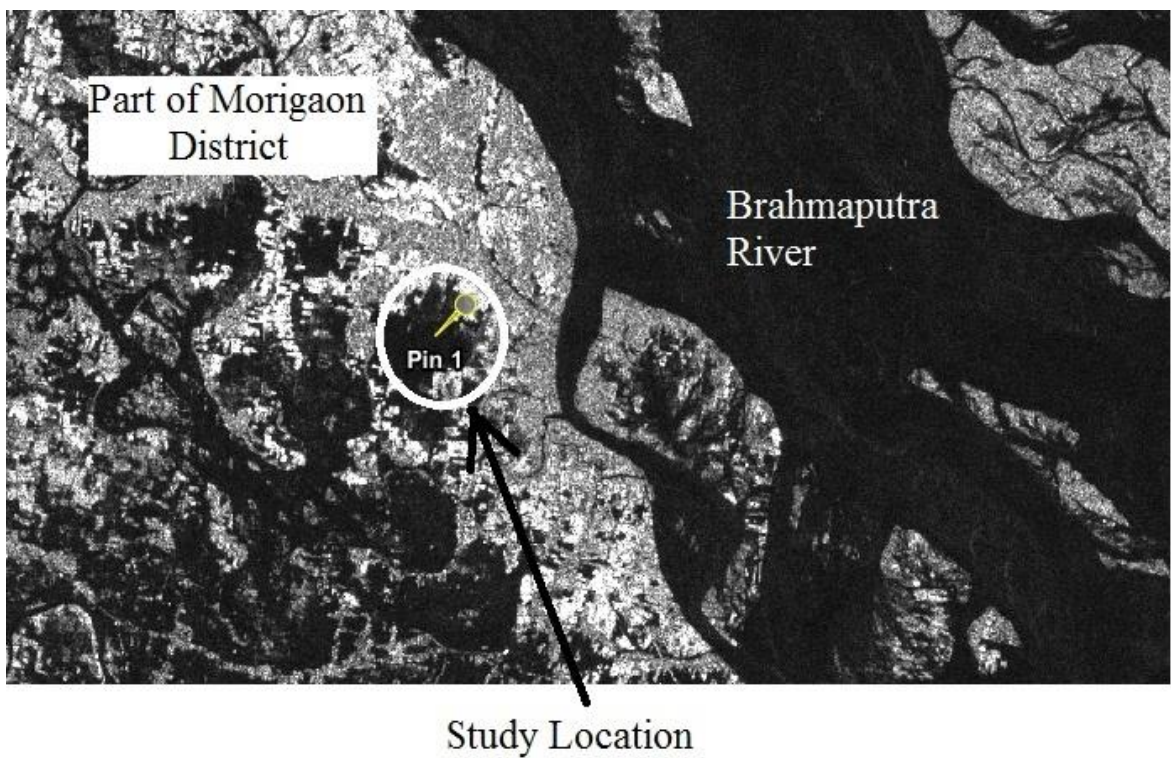


Figure 4.31: Study area during flooding on 14th July 2017 as seen in a VV SAR image

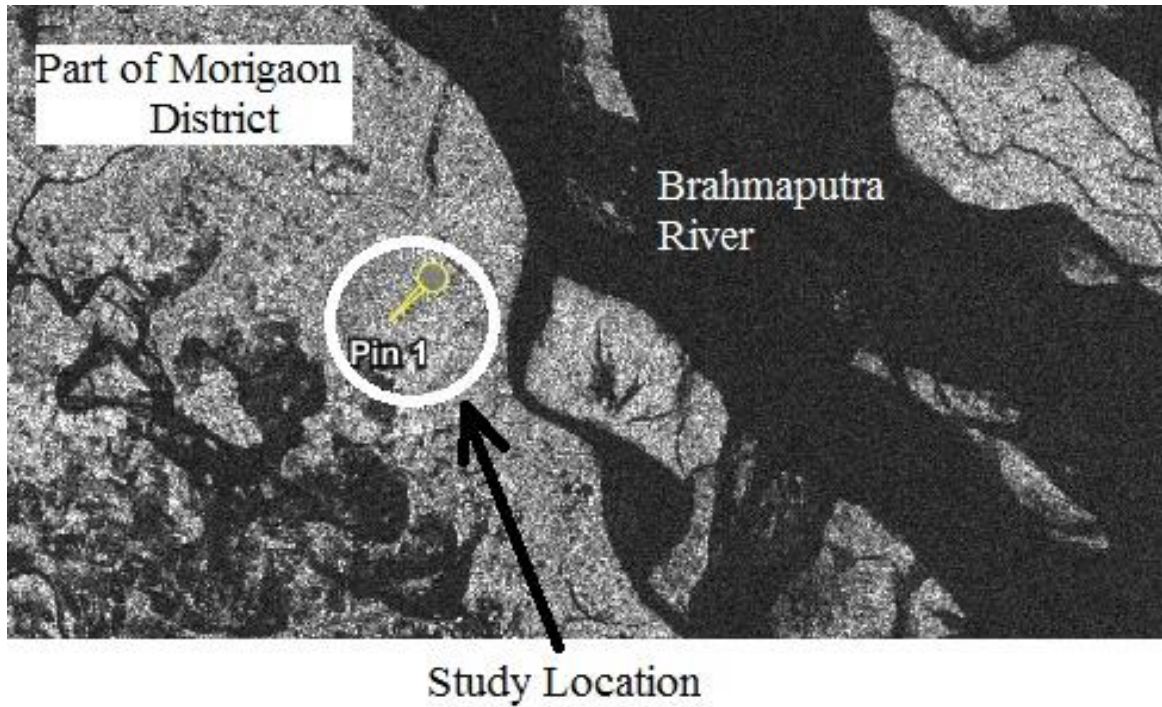


Figure 4.32: Study area after the occurrence of flood on 26th July 2017 as seen in a VH SAR image

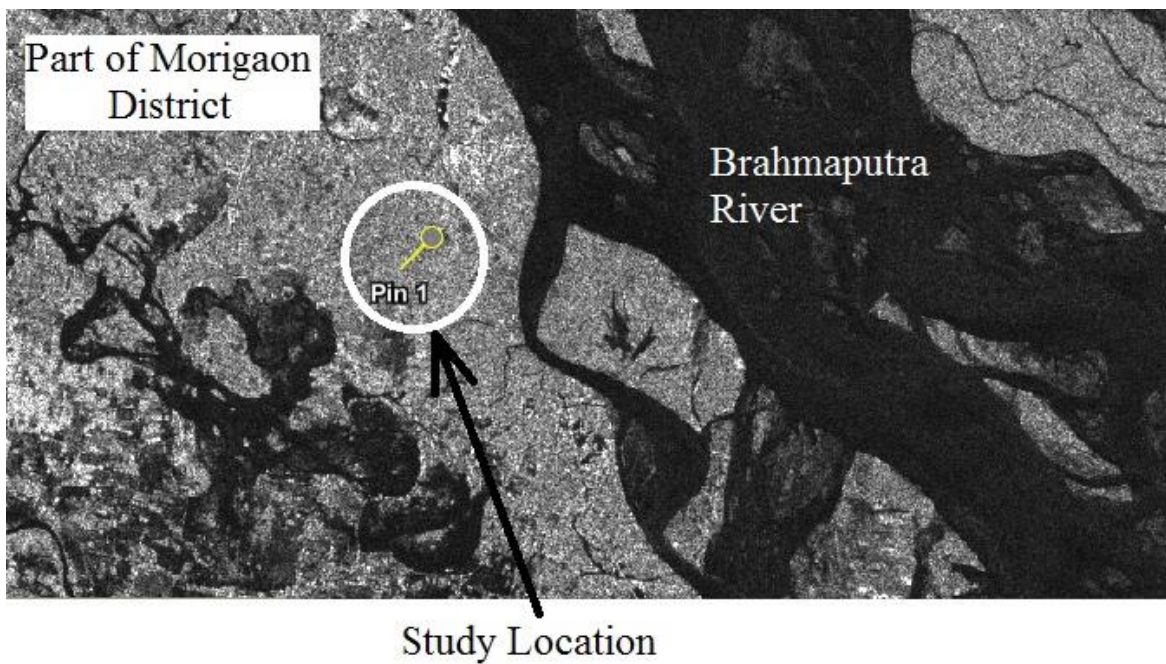


Figure 4.33: Study area after the occurrence of flood on 26th July 2017 as seen in a VV SAR image

During the flooding day of 14th of July 2017, the scattering coefficient variation in the boundary pixels of the study location is observed in all possible directions, such as, horizontal boundary, vertical boundary and angular boundary. Also, the variation of scattering coefficient value at the centre of the flood is observed. Finally a comparison of the results is done. The Figure 4.34 shows the boundary pixels taken into consideration in different directions for the flooded area.

The variations of backscattering coefficient values for all the boundary regions are plotted and compared with high resolution Bhuvan flood images for validation purpose as explained in the following sub-section.

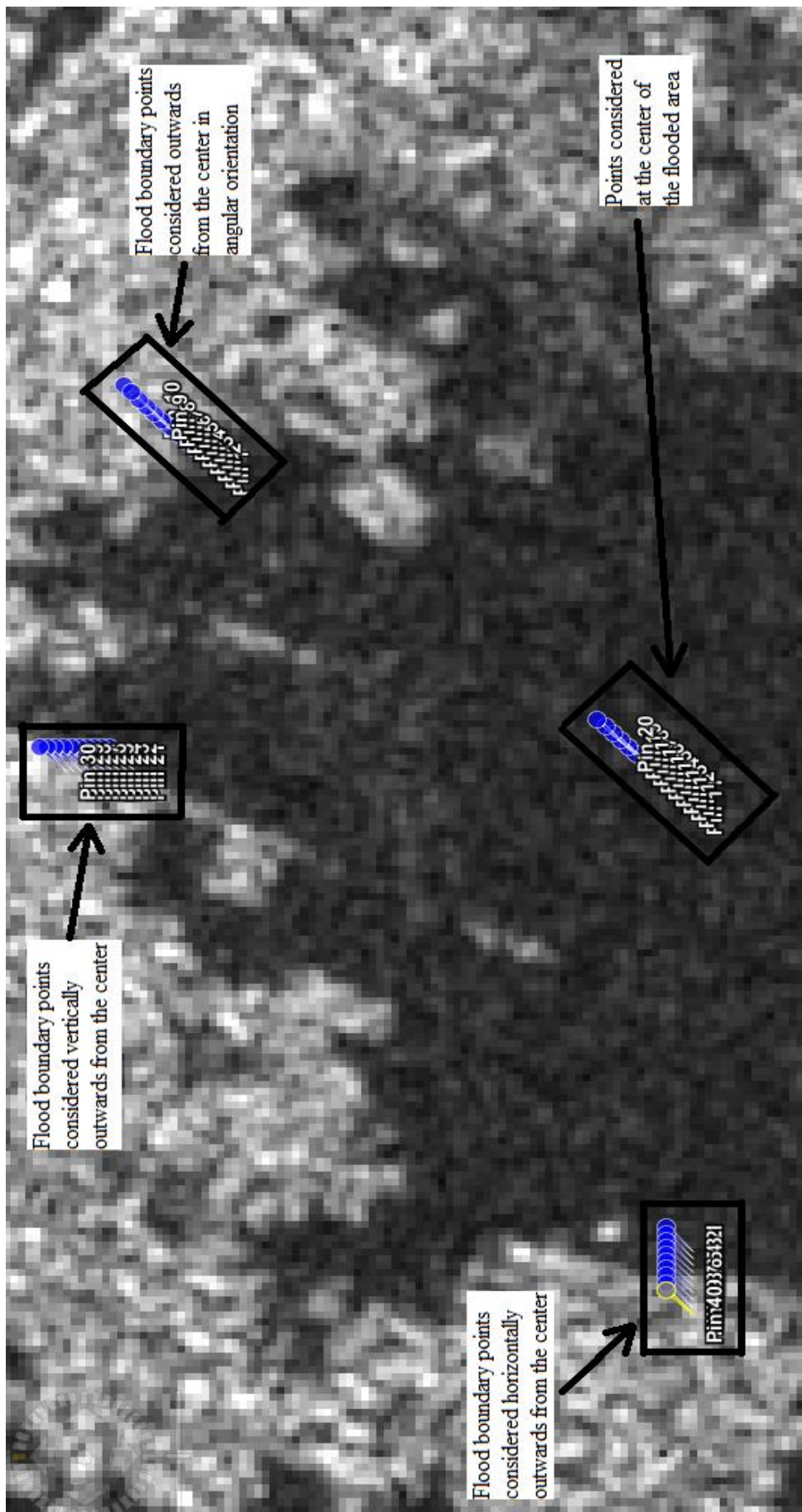


Figure 4.34: Boundary pixels for studying scattering coefficient variation in all directions

4.6.7 Validation of the experimental results

Figure 4.35 shows the Bhuvan image of the same area as experimented with for flood boundary delineation on 14th July 2018. The flooded portion of the study area is shown in light blue coloured patches in the image.

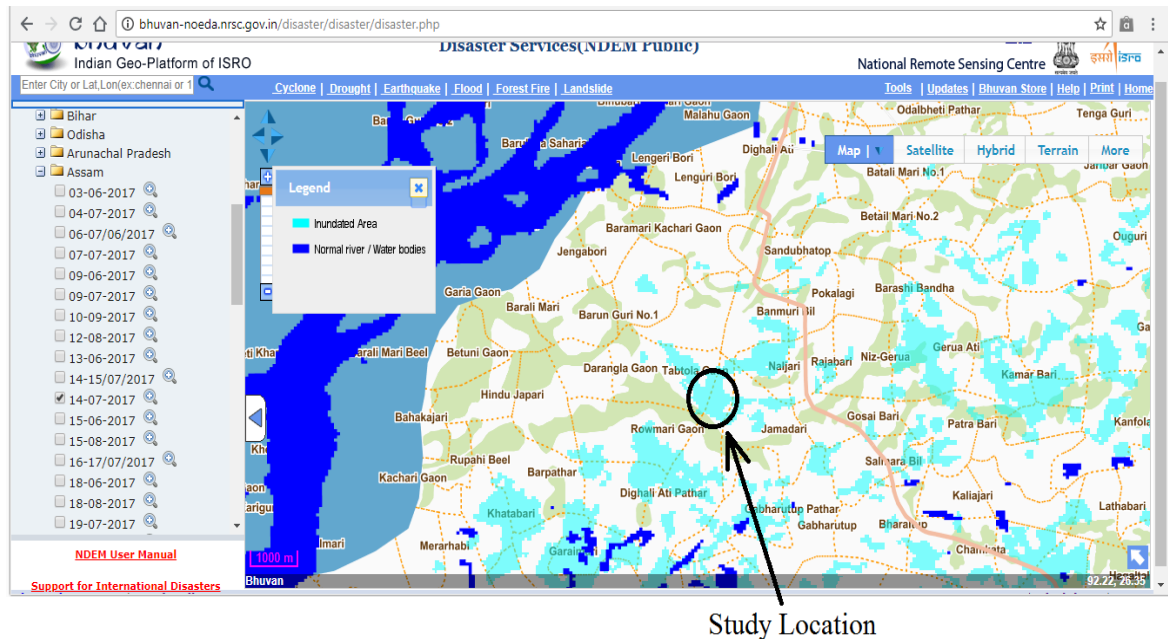


Figure 4.35: The study location being flooded as on 14th July 2017 [Source of the image: <http://bhuvan-noeda.nrsc.gov.in/disaster/disaster/disaster.php>]

Figures 4.36 to 4.39 show the variations of backscattering coefficient values in different directions of the flooded area. The figures show the increase in scattering coefficient values from inside the flooded area to outside it. This is mainly due to gradual change in water content of the targeted area along the border, from 100% inside the flooded area (fully submerged in water due to flood) to as low as 20% of soil moisture (away from the flooded area). Thus the scattering coefficient also varies from a low value (~20) to a very high value (~140). Thus it is observed that flood boundary in any direction can be found, by observing the variation of backscattering coefficient value along that direction. This is validated by comparing the results with Bhuvan flood maps.

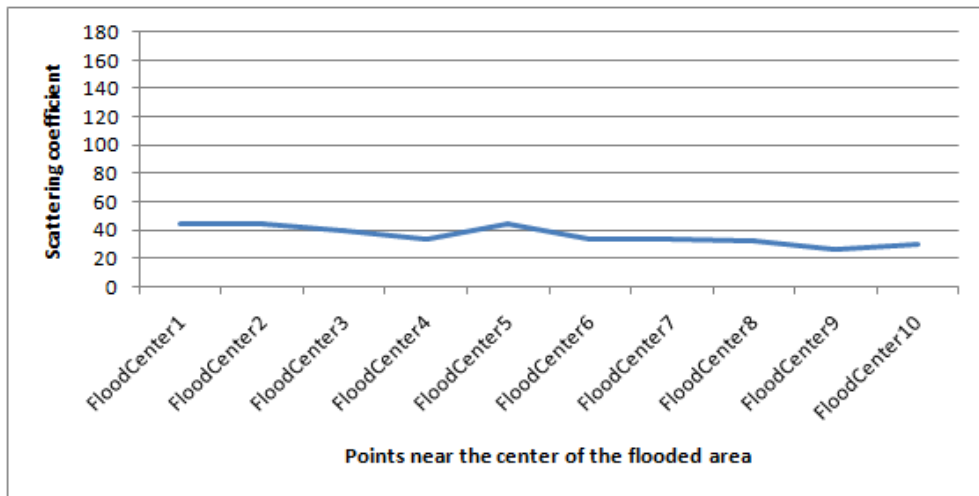


Figure 4.36: Variation of backscattering coefficient inside the flooded area

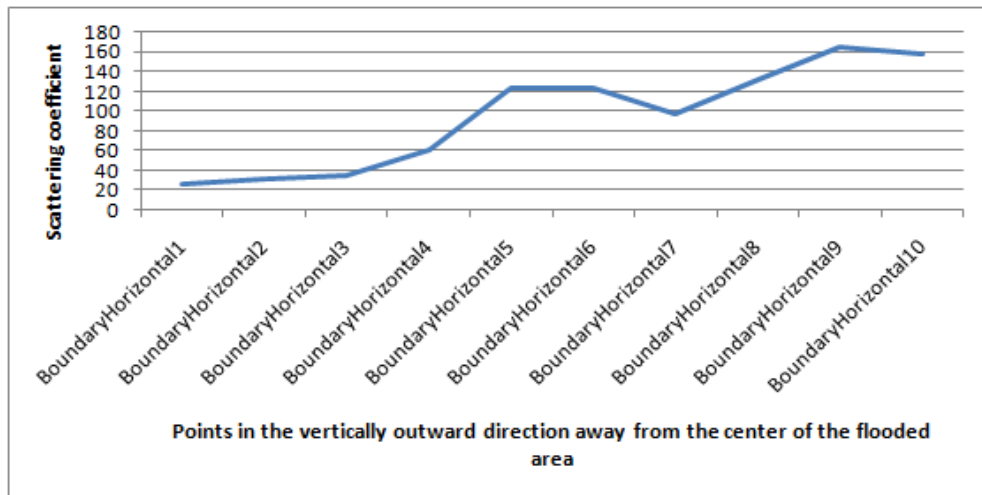


Figure 4.37: Variation of backscattering coefficient horizontally in the flood boundary

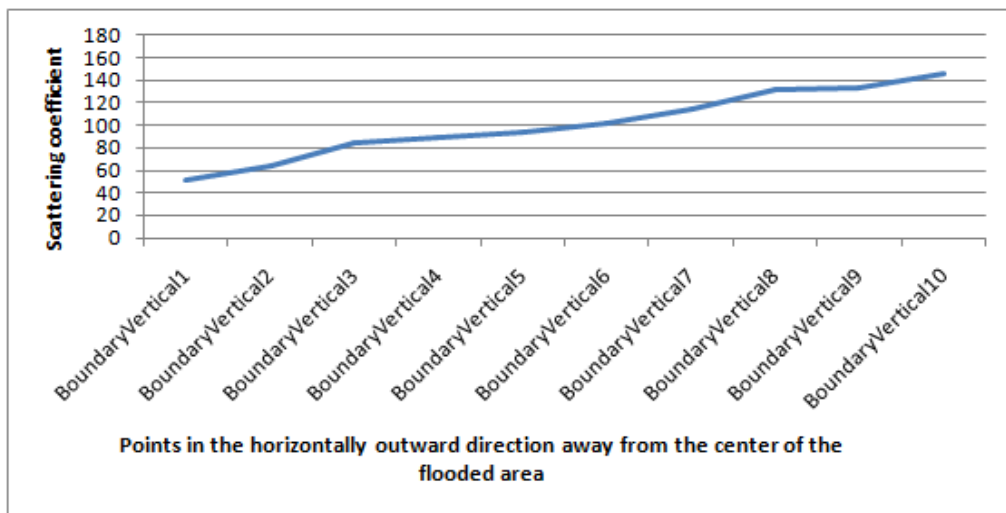


Figure 4.38: Variation of backscattering coefficient vertically in the flood boundary

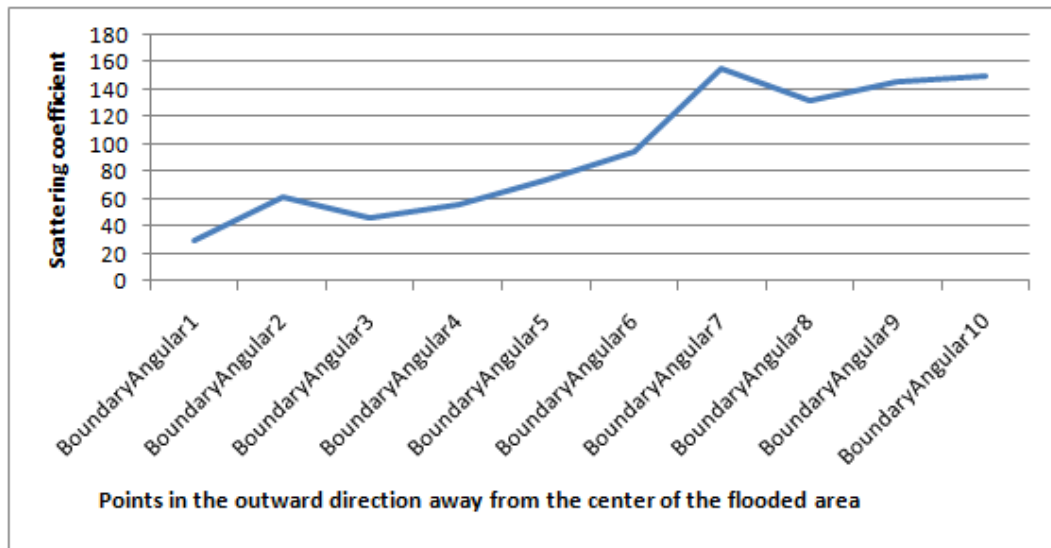


Figure 4.39: Variation of backscattering coefficient in the flood boundary in angular direction

The above figures show the variations of the backscattering coefficient values measured from the SAR images. The variations observed are listed in the following.

1. The variation of backscattering coefficient from inside the flooded area to outside it is gradually increasing in value.
2. The slope of the variation from inside the flooded area to outside it in all directions is positive.
3. The slope of the variation depends on various factors, such as- soil type, soil moisture content, existing open water bodies, land cover types etc.
4. The slope is not same in all cases, but the presence of a steep slope is a common phenomenon in the boundary of a flooded area.

4.6.8 Inferences

It is observed from the above discussion that if the scattering coefficient measurement of a flooded area shows an increasing trend in a particular direction, that would indicate the boundary of the flooded area in that direction. In both VH and VV polarisations this change is observed. Hence, it can be concluded that SAR image in C-

band in either VH or VV polarization can be used in flood boundary delineation and monitoring.

4.7 CHAPTER CONCLUSIONS

This chapter presented the passive as well as active microwave remote sensing methods useful for places having-

- (a) Large open water bodies
- (b) High soil moisture
- (c) Extensive vegetation

The exact nature of the methods developed with their performance characteristics are shown in summarised form in the following.

- (1) Brightness Temperature difference in Vertical Polarization- this is a new method developed, with a spatial resolution of 25 km x 25 km, accuracy level being 70 percent.
- (2) Brightness Temperature ratio with Threshold value- Introduction of the concept of Threshold value in the ratio is done for the first time. The spatial resolution is 25 km x 25 km. The accuracy level is slightly more than 70 percent.
- (3) Polarization Index- The use of this index in flood detection and monitoring is done for the first time. Earlier use was in soil moisture measurement. The resolution is 10 km x 10 km. The accuracy level is about 80 percent.
- (4) SAR Scattering Coefficient- Use of C-band scattering coefficient is done successfully for the first time in flood detection and monitoring, as well as in delineation of flood boundary. The spatial resolution is 5 m x 5 m. The accuracy of the method is about 90 percent.